UC San Diego

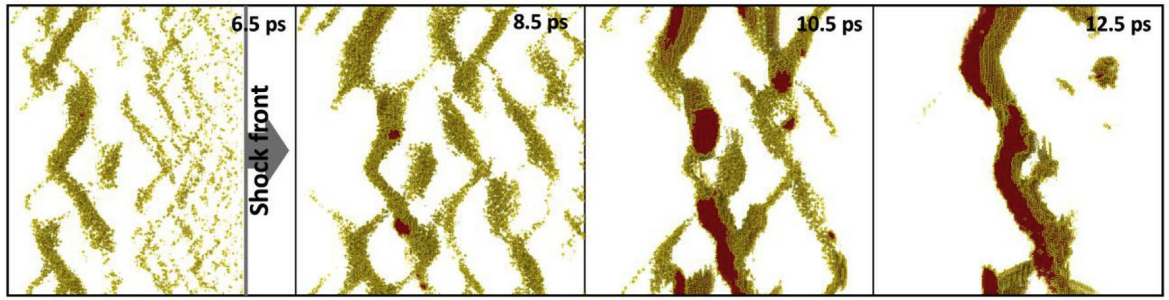

Amorphization in materials

Literature Review

Boya Li

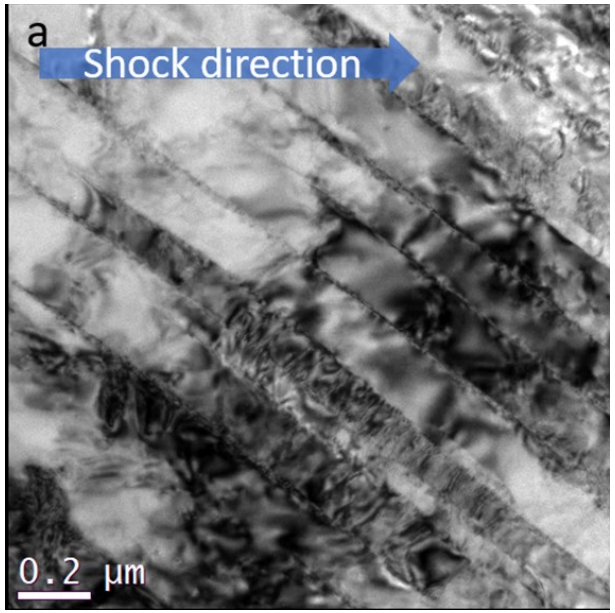

Committee:

Dr. Marc Meyers (chair)

Dr. Vlado Lubarda

Dr. Javier Garay

Dr. Vitali Nesterenko

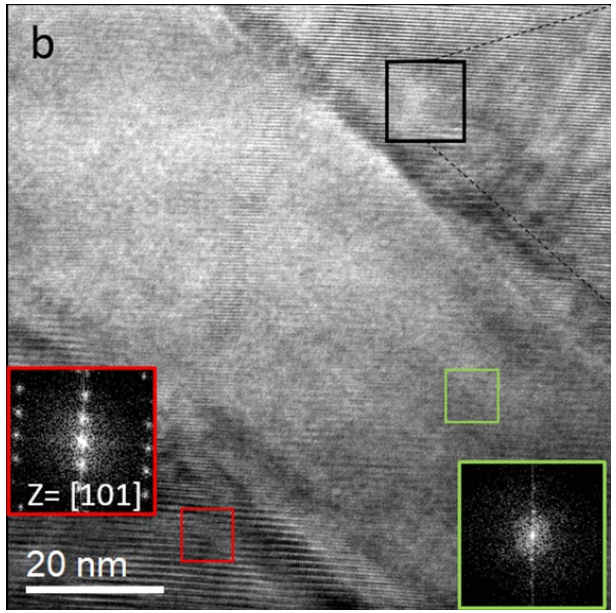

States of matter

The state of atomic motion

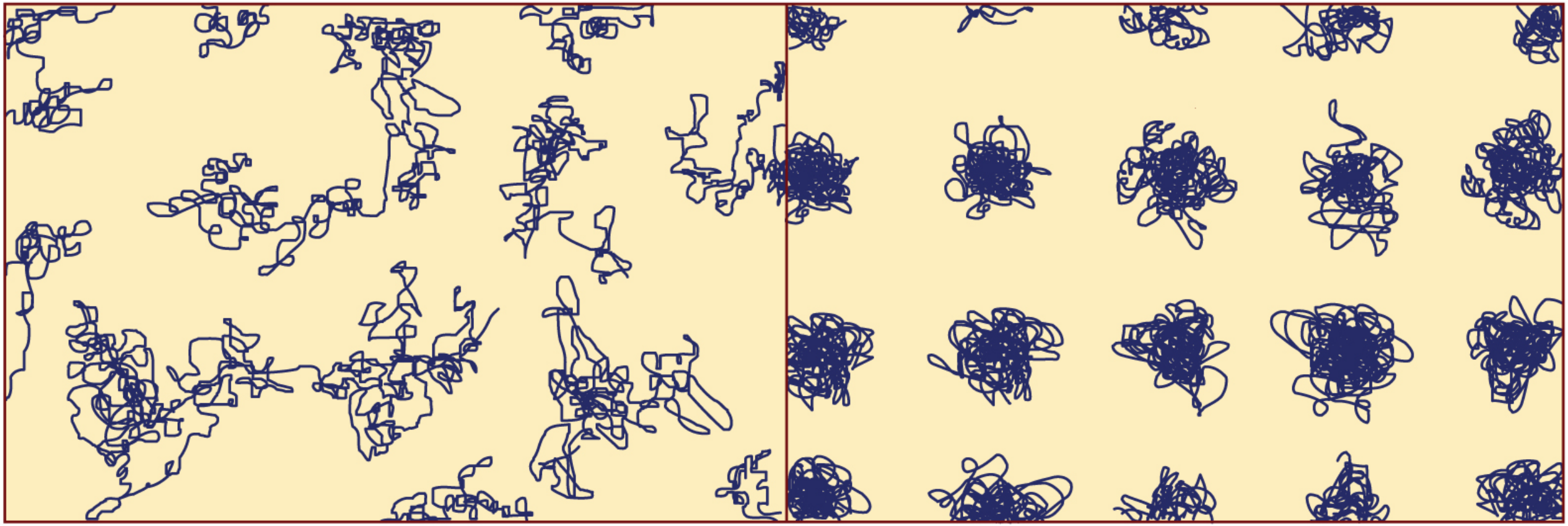

liquid

solid

Crystalline and amorphous solids

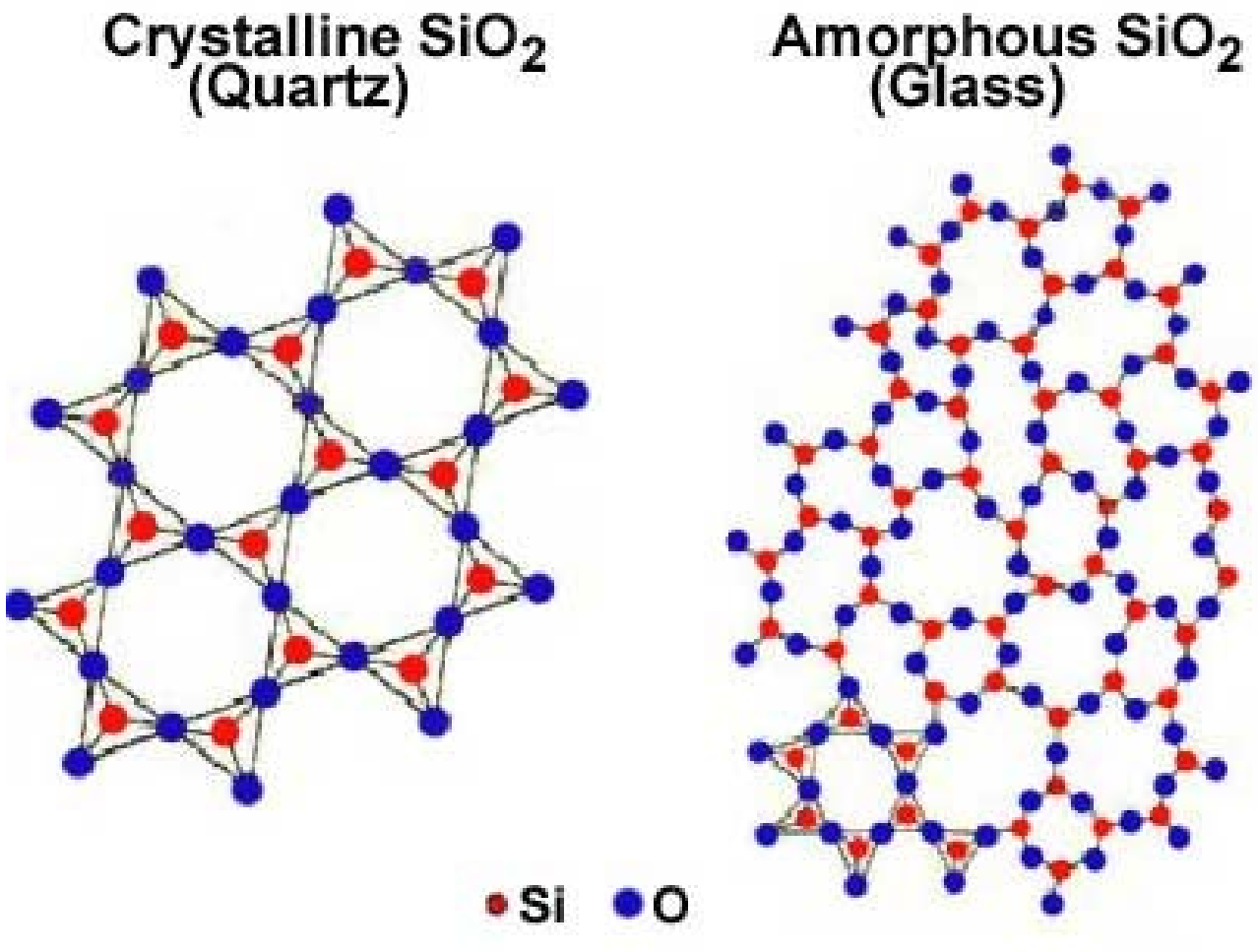

Amorphization exists in a variety of materials

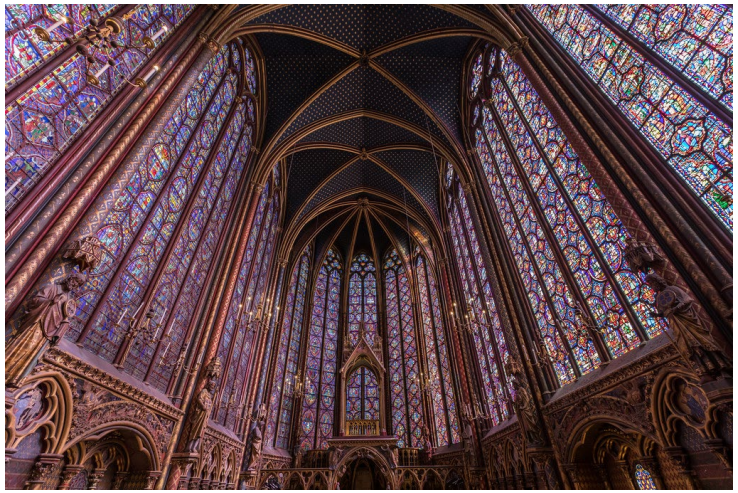

Amorphous solids vs. length scale

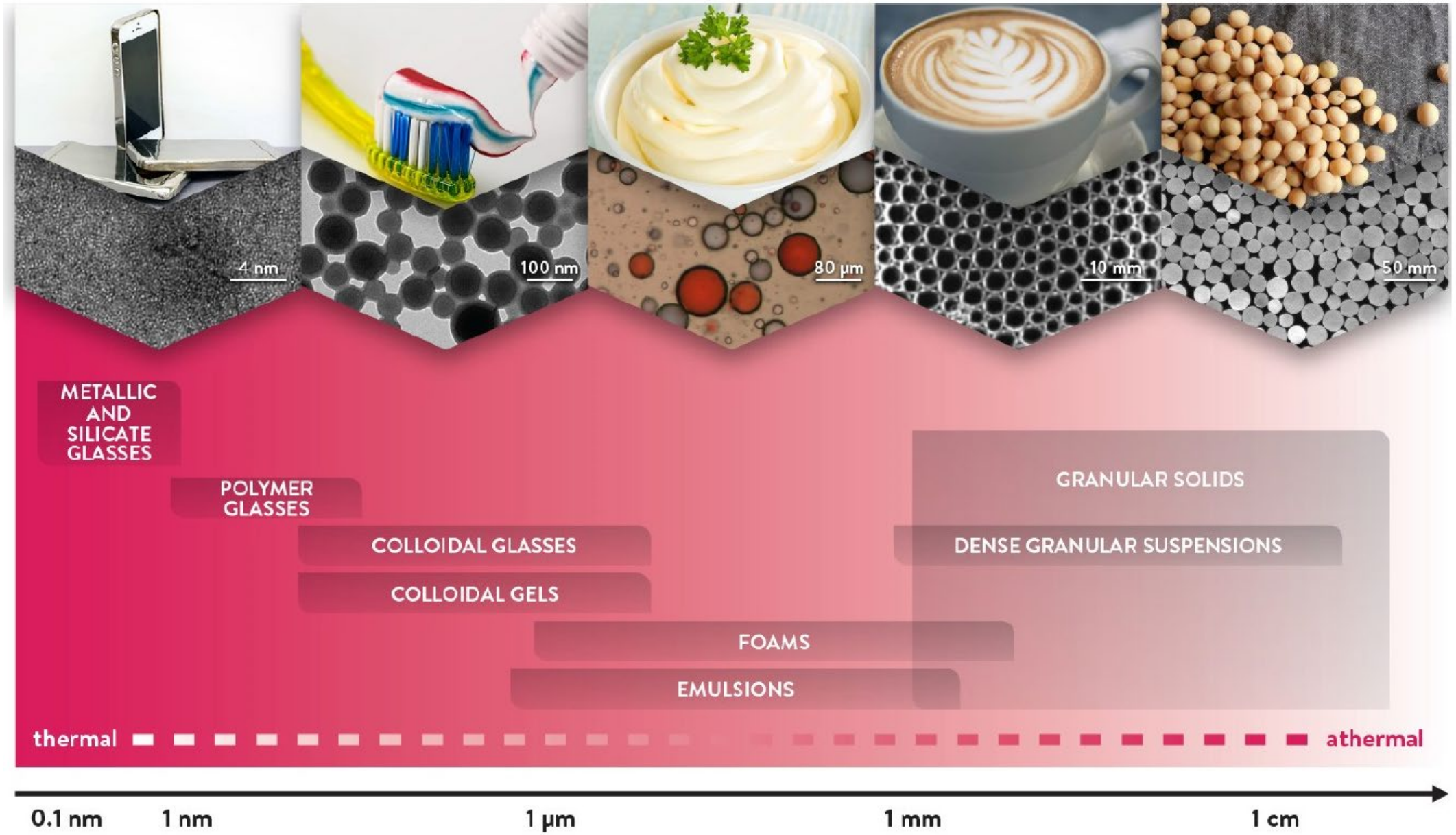

Nicolas et al, Reviews of Modern Physics, 2018

Crystalline	Amorphous	Liquid
Regular repeating pattern	No pattern	No pattern
Unit cell	No unit cell	No unit cell
Fixed shape	No fixed geometrical shape	No fixed geometrical shape
Liquid cooled slowly → crystal	Liquid cooled quickly → amorphous (super cooled liquid)	--
Sharp melting point	No sharp melting point (within a long range)	--
Axis or plane of symmetry	No symmetry	No symmetry
Anisotropic	Isotropic	Isotropic
Fixed cleavage plane to break along	No cleavage planes	--
Definite heat of fusion	Indefinite heat of fusion due to absence of sharp melting point	--
Atoms/molecules are not free to move, no random motion	Atoms/molecules are not free to move, no random motion	Atoms/molecules are free to move, random motion

Melting of crystals- first order phase transition

A first-order phase transition-a discontinuous change in the properties of the material, such as density.

https://aatishb.com/entropy/

Forming of glass

https://www.youtube.com/watch?v=gadvVvIEEkc

Amorphous metals/metallic glasses

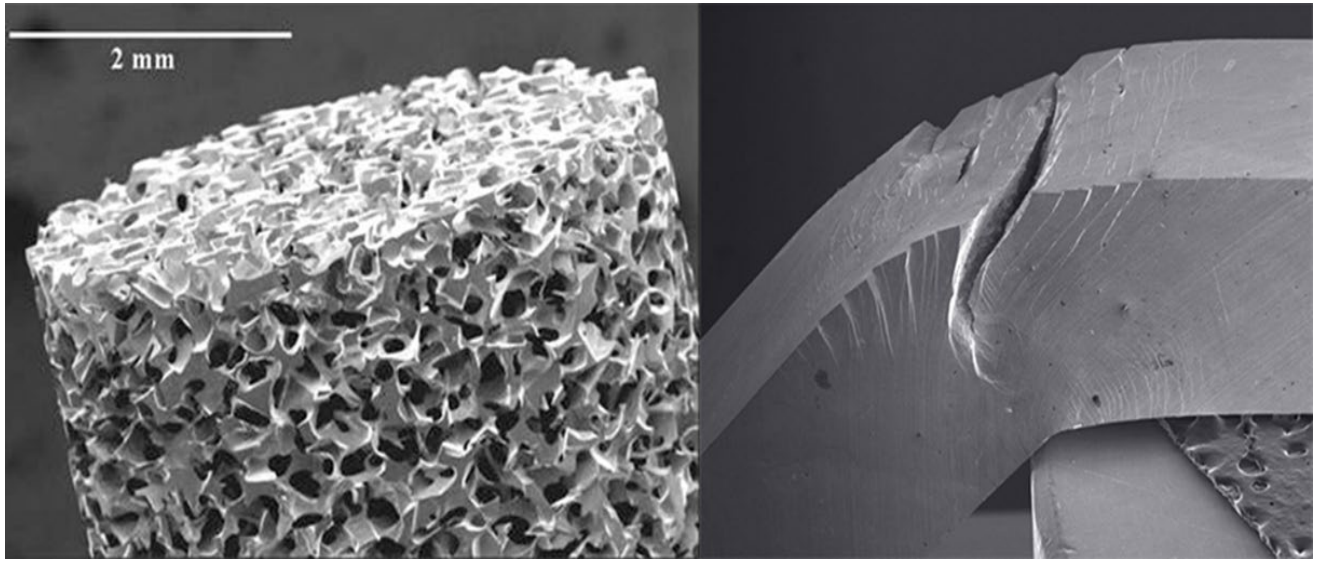

Puiu, ZME Science, 2020

Amorphous metals/metallic glasses

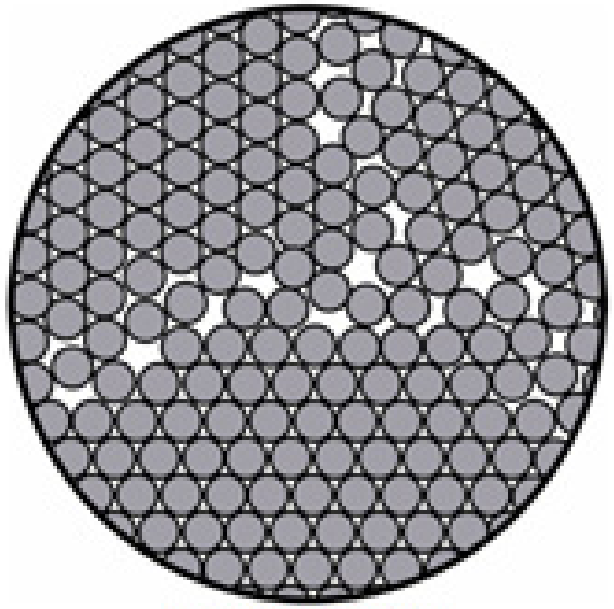

Most Metals

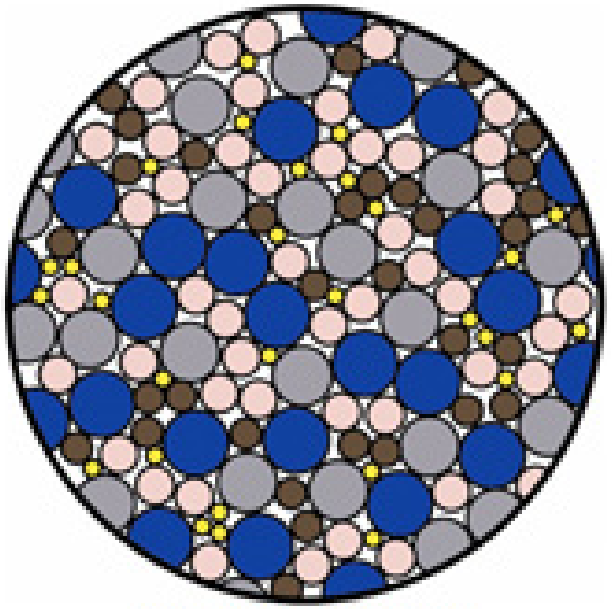

Metallic Glass

Dr. Pol Duwez

- Belgian-American scientist
- First created amorphous metal by rapid cooling method at Caltech in 1957

- Polycrystalline grains of varying shapes and sizes
- Misaligned planes of atoms slip past each other easily, absorbing energy and allowing dislocations to move, making deformation permanent
- Grain boundaries represent weak spots

- Cooled faster than atoms can rearrange into a crystal
- Dislocation movement obstructed so absorbs less energy and rebounds elastically to its initial shape
- Resistant to corrosion and wear
- Slow heat conduction limits casting

Ashby plot comparing several materials classes

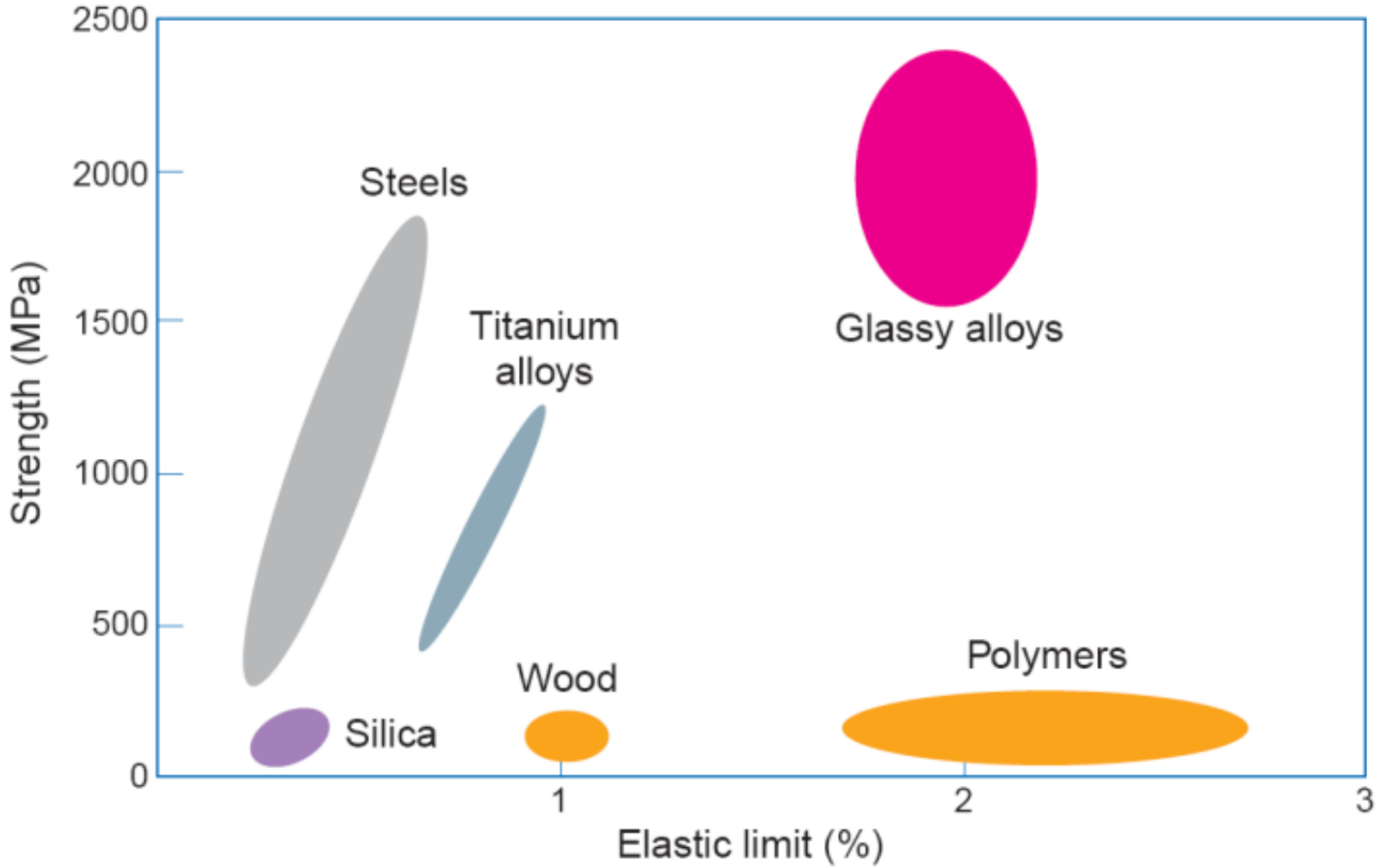

- much stronger and less brittle than oxide glasses and ceramics
- higher tensile yield strengths and higher elastic strain limits than polycrystalline metal alloys
- but at ambient temperatures they exhibit very little plasticity before failure through shear localization

Homer, Dissertation, 2010

The basic properties of different Bulk Metallic Glasses (BMGs)

Base metal	Properties based on the base metal
Fe-based	Soft magnetism (glass, nanocrystal) Hard magnetism (nanocrystal) High corrosion resistance High endurance against cycled impact deformation
Co-based	Soft magnetism (glass, nanocrystal) Hard magnetism (nanocrystal) High corrosion resistance High endurance against cycled impact deformation
Ni-based	High strength, high ductility High corrosion resistance High hydrogen permeation
Cu-based	High strength, high ductility (glass, nanocrystal) High fracture toughness, high fatigue strength High corrosion resistance
Pd-based	High strength High fatigue strength, high fracture toughness High corrosion resistance

Patel et. al, IntechOpen, 2020

Composition and properties of different types of BMGs

Base metal	Metal–Metalloids	Metal–Metal
Fe-based	Fe–(Al,Ga)–(P,C,B,Si) Fe–Ga–(P,C,B,Si) Fe–Ga–(Nb,Cr,Mo)–(P,C,B) (Los Alamos) Fe–(Cr,Mo)–(B,C) Fe–(Zr,Hf,Nb,Ta)–B Fe–(B,Si)–Nb	Fe–Nd–Al
Co-based	Co–Ga–(Cr,Mo)–(P,C,B) Co–(Zr,Hf,Nb,Ta)–B Co–Ln–B	Co–Nd–Al Co–Sm–Al
Ni-based	Ni–(NbCr,Mo)–(P,B) Ni–(Ta,Cr,Mo)–(P,B) Ni–Zr–Ti–Sn–Si (Yonsei University) Ni–Pd–P	Ni–Nb–Ti Ni–Nb–Zr Ni–Nb–Hf Ni–Nb–Zr–Ti Ni–Nb–Zr–Ti–M (M = Fe, Co, Cu) Ni–Nb–Hf–Ti Ni–Nb–Hf–Ti–M Ni–Nb–Sn (Cal Tech)

Patel et. al, IntechOpen, 2020

Cont. table

Base metal	Metal–Metalloids	Metal–Metal
Cu-based	Cu–Pd–P Cu–Ni–Pd–P	Cu–Zr–Ti Cu–Hf–Ti Cu–Zr–Ti–Ni Cu–Hf–Ti–Ni Cu–Zr–Ti–Y Cu–Hf–Ti–Y Cu–Zr–Ti–Be Cu–Hf–Ti–Be Cu–Zr–Al Cu–Hf–Al Cu–Zr–Al–M Cu–Hf–Al–M (M = Ni, Co, Pd, Ag) Cu–Zr–Ga Cu–Hf–Ga Cu–Zr–Ga–M Cu–Hf–Ga–M Cu–Zr–Al–Y (Cal Tech)
Pd-based	Pt–Cu–P Pt–Cu–Co–P (Cal Tech) Pt–Pd–Cu–P	

Patel et. al, IntechOpen, 2020

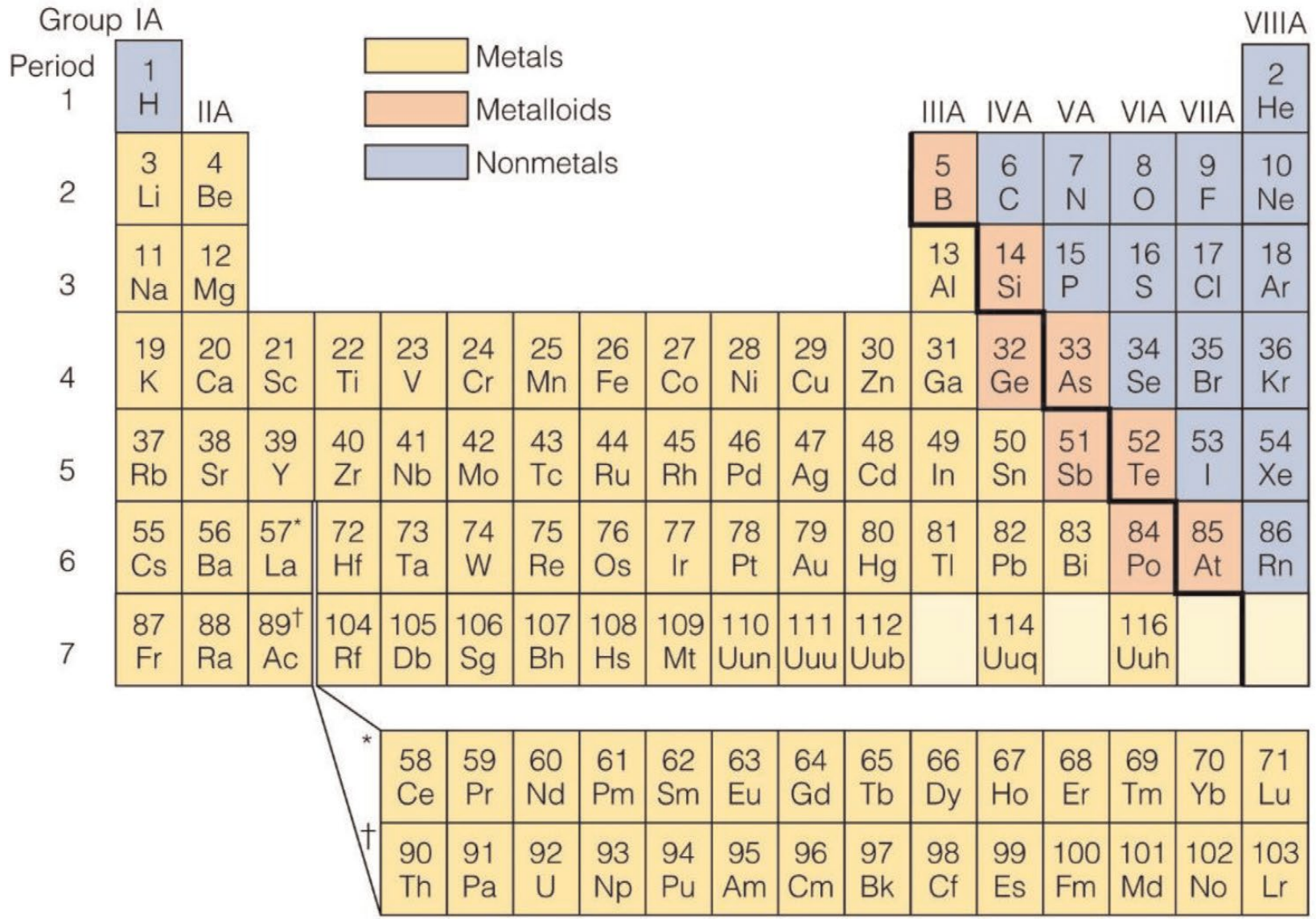

Metal-metal MG:

- "Sea" of electrons
- Coulombic interactions between delocalized valence electrons and positively charged ionized cores

Metal-metalloid MG:

- Metalloid elements
- Ionic and/or covalent bonding
- Relative amounts of covalent bonding: indicated by chemistry and equilibrium (crystalline) phases

Processing of metallic glasses

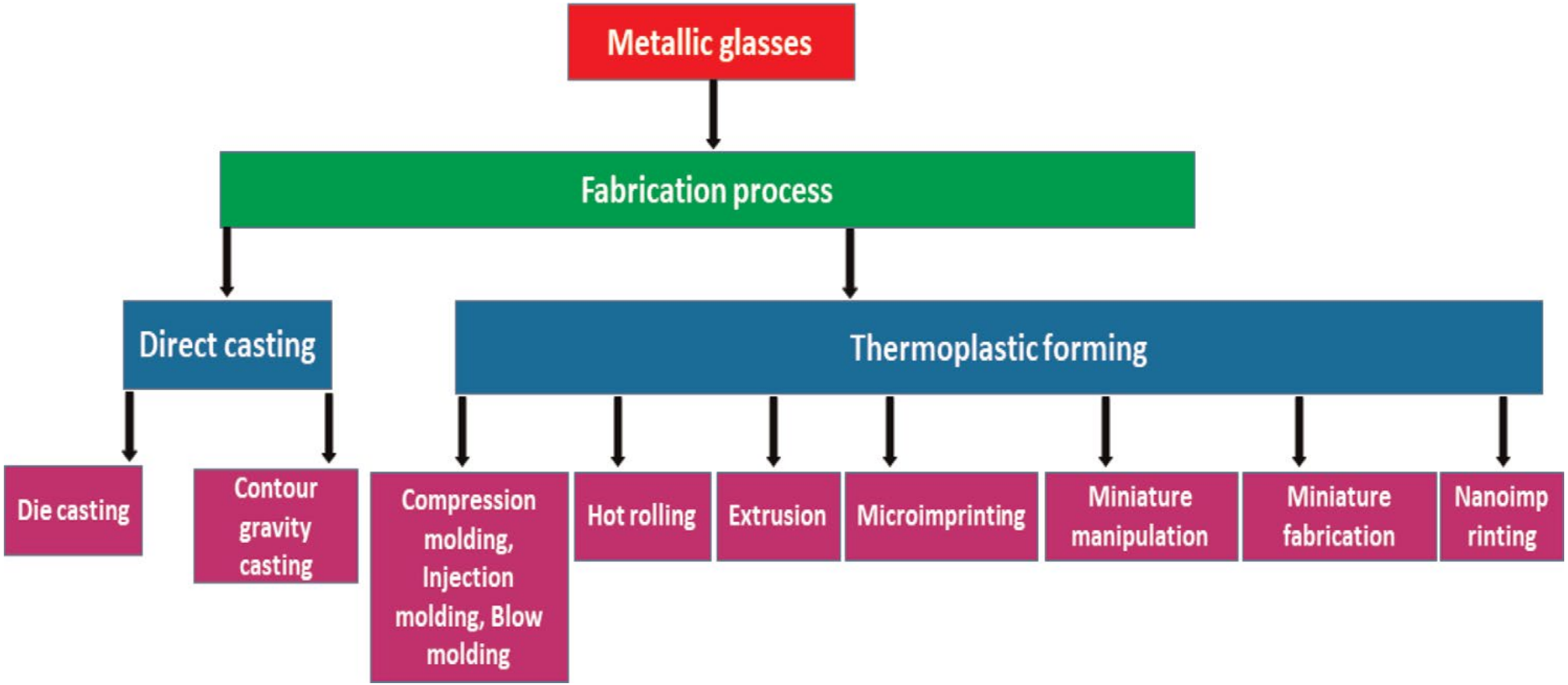

Patel et. al, IntechOpen, 2020

Structure of amorphous metals

- Random mixture of metallic and metalloid atoms
- No long-range-order, short range is defined as the first- or second-nearest neighbors of an atom
- There exists short-range-order (clusters) and medium-range order (extended clusters)

Cluster Model

- Atomic clusters: short-range order (SRO)

Common clusters that exist in amorphous metals:

Tricapped trigonal prism
CN=9

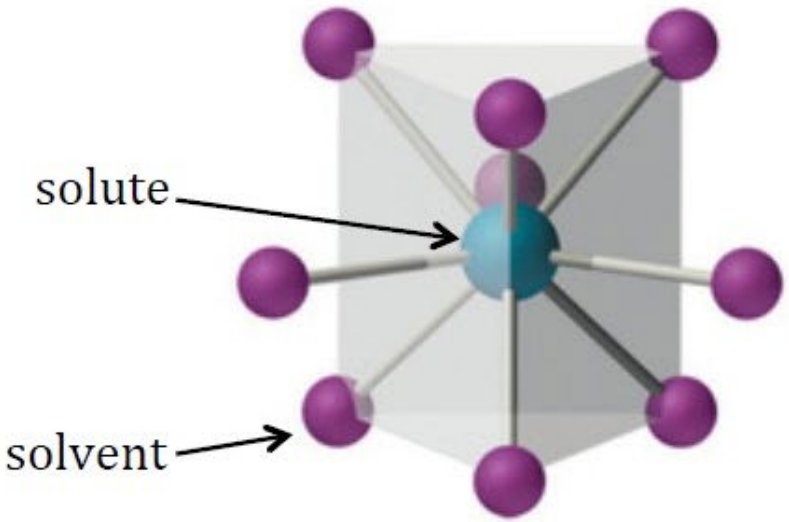

Icosahedron
CN12

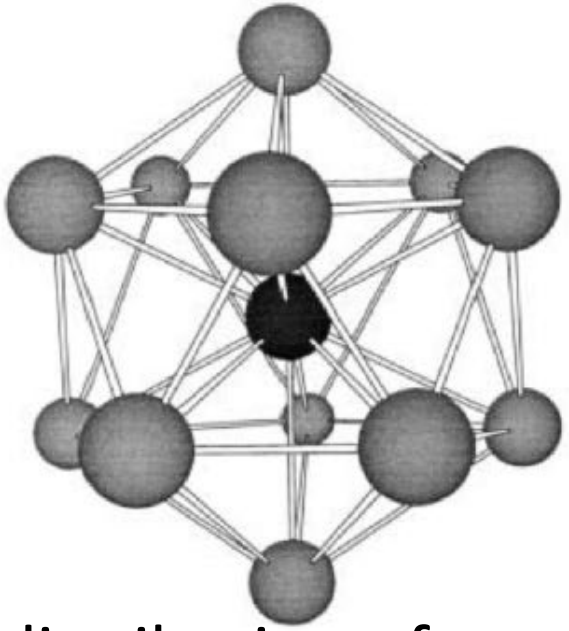

Coordination number of solute atom varies with distribution of atomic size ratio in calculations of representative metals

Extended Cluster Model

- Extended clusters:
  medium-range order (MRO)

When solute concentration increases, more solute connections form in extended clusters or strings 1-2 D connectivity

CN of solutes in strings is normally 3-7

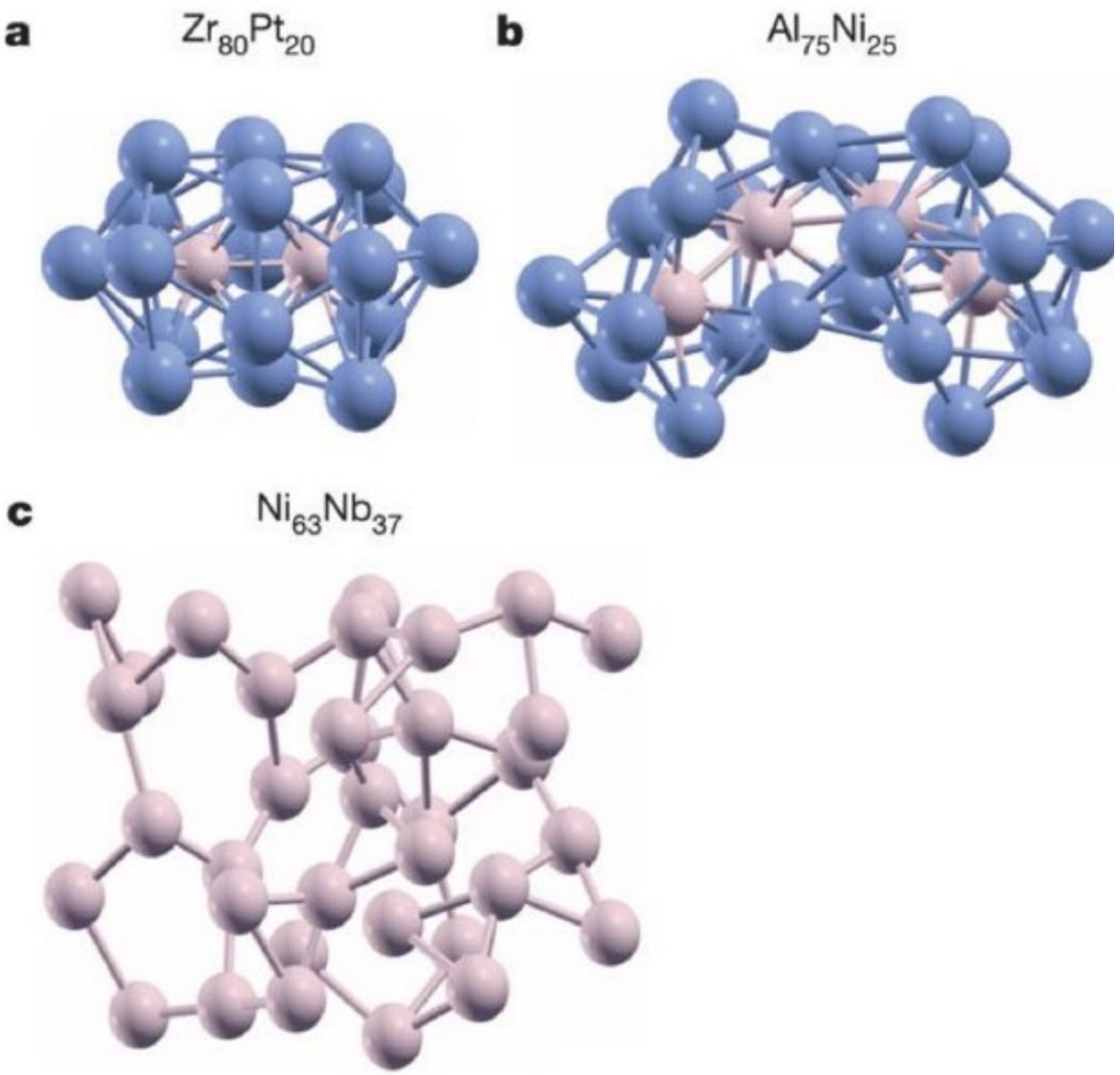

Sheng et.al Nature, 2006

Comparison of different amorphous structures

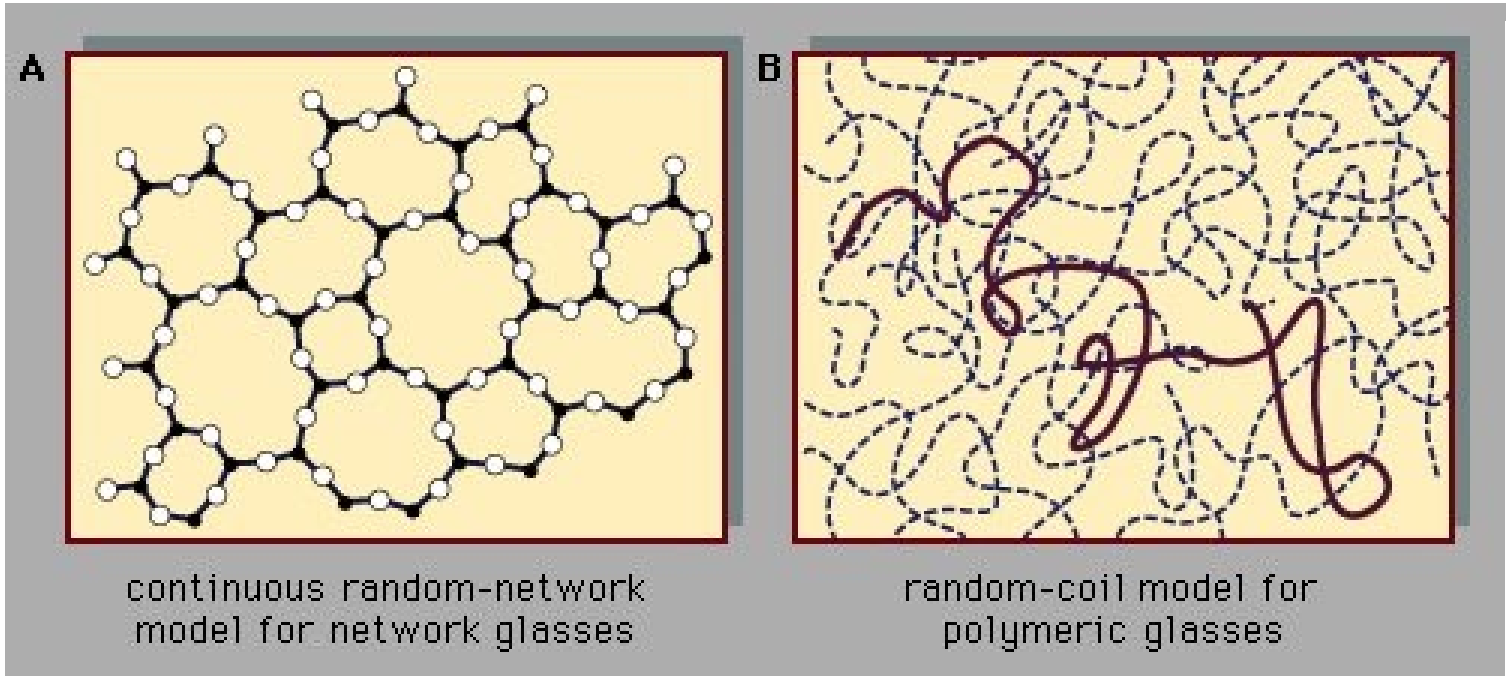

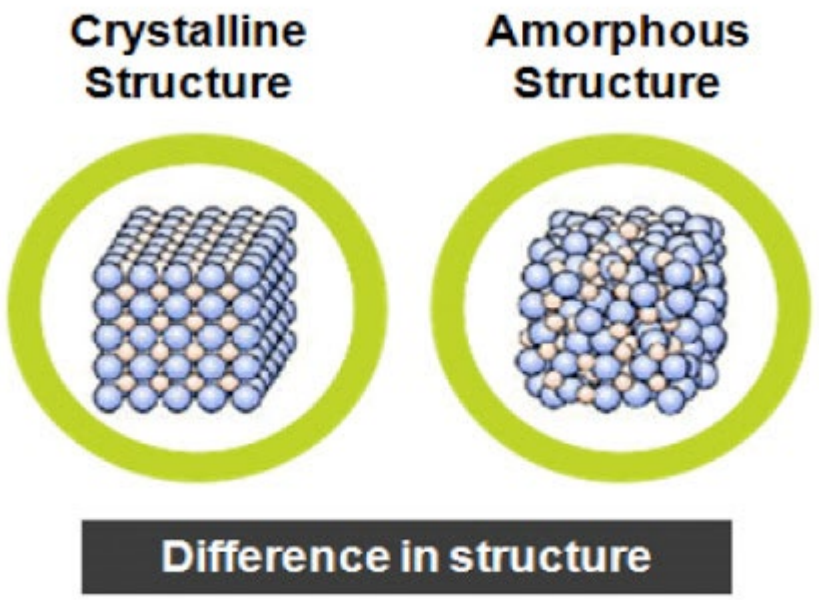

(1) The continuous random-network model for covalently bonded glasses, such as amorphous silicon and oxide glasses
(2) The random-coil model for many polymer-chain organic glasses, such as polystyrene
(3) The random close-packing model for metallic glasses, which is like a bunch of marbles are swiftly scrunched together in a bag.

Zachariasen random network theory

Network structure of silicate (SiO_4^{4-}) tetrahedrons

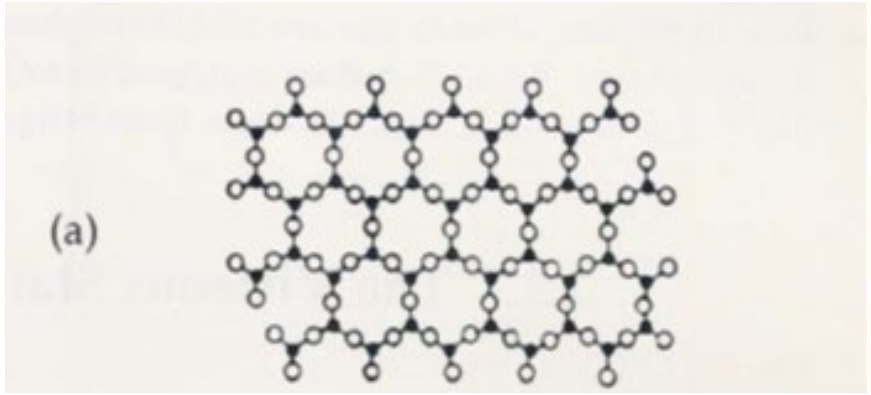

Quartz crystal

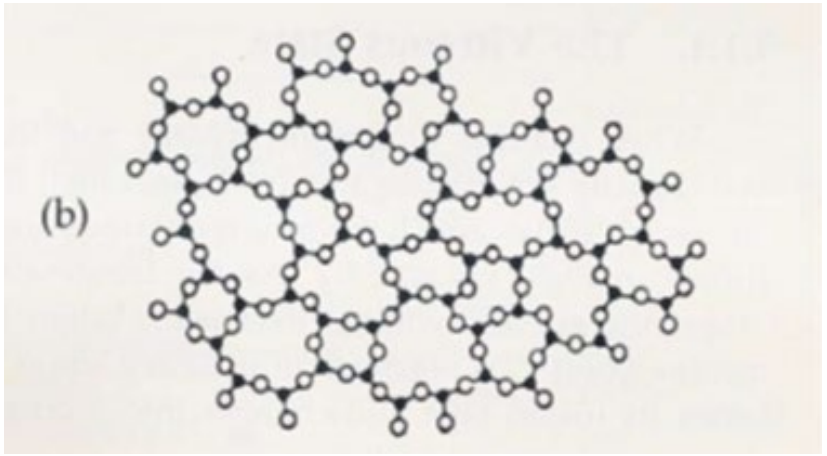

Quartz glass

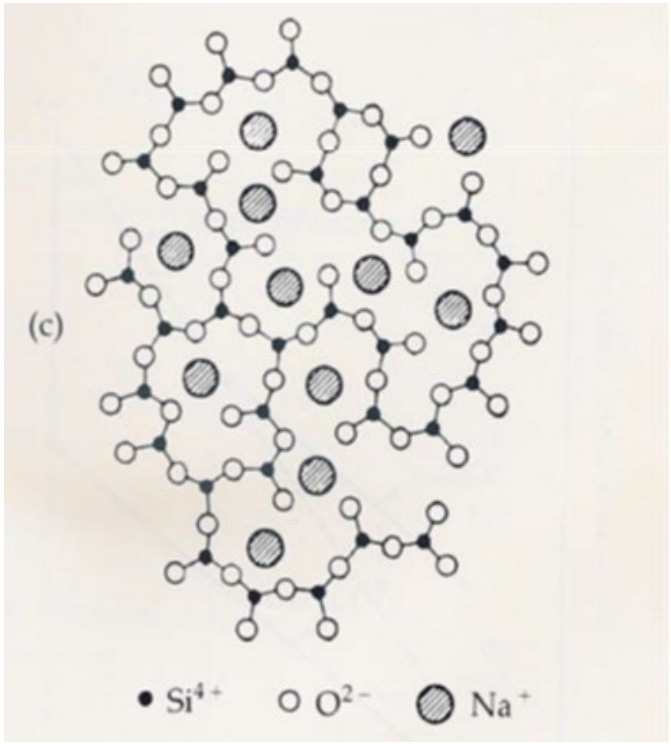

Sodium silicate glass

The four rules for the formation of a glass from an oxide A_mO_n are:

- No oxygen atom may be linked to more than two cations
- The cation coordination number is small: 3 or 4.
- Oxygen polyhedra share corners, not edges or faces.
- For 3D networks, at least three corners must be shared

T.S. Izumitani, Optical glass, 1986

Comparison with gas

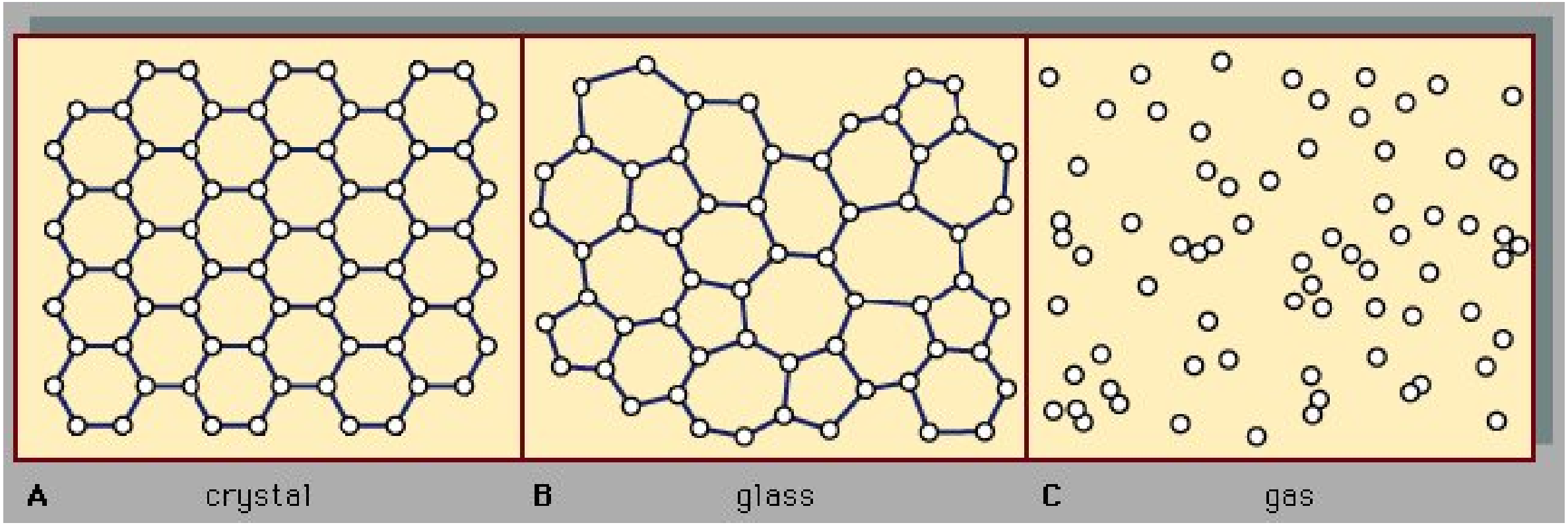

In crystal (A) and glass (B), solid dots denote the fixed points about which the atoms oscillate, lines denote the chemical bonding between atoms

In gas (C), dots denote a snapshot of one configuration of instantaneous atomic positions

(A) long-range order or translational periodicity; positions repeat in space in a regular array

(B) Translational periodicity is absent, no long-range order. The atoms are not randomly distributed in space as they are in the gas in (C).

Bonding types and glass transition temperatures of representative amorphous solids

Glass	bonding	glass transition temperature (K)
silicon dioxide	covalent	1,430
germanium dioxide	covalent	820
silicon, germanium	covalent	—
40% palladium, 40% nickel, 20% phosphorus	metallic	580
beryllium difluoride	ionic	570
arsenic trisulfide	covalent	470
polystyrene	polymeric	370
selenium	polymeric	310
80% gold, 20% silicon	metallic	290
water	hydrogen-bonded	140
ethanol	hydrogen-bonded	90
isopentane	van der Waals	65
iron, cobalt, bismuth	metallic	—

Glass formation from liquid- second-order phase transition

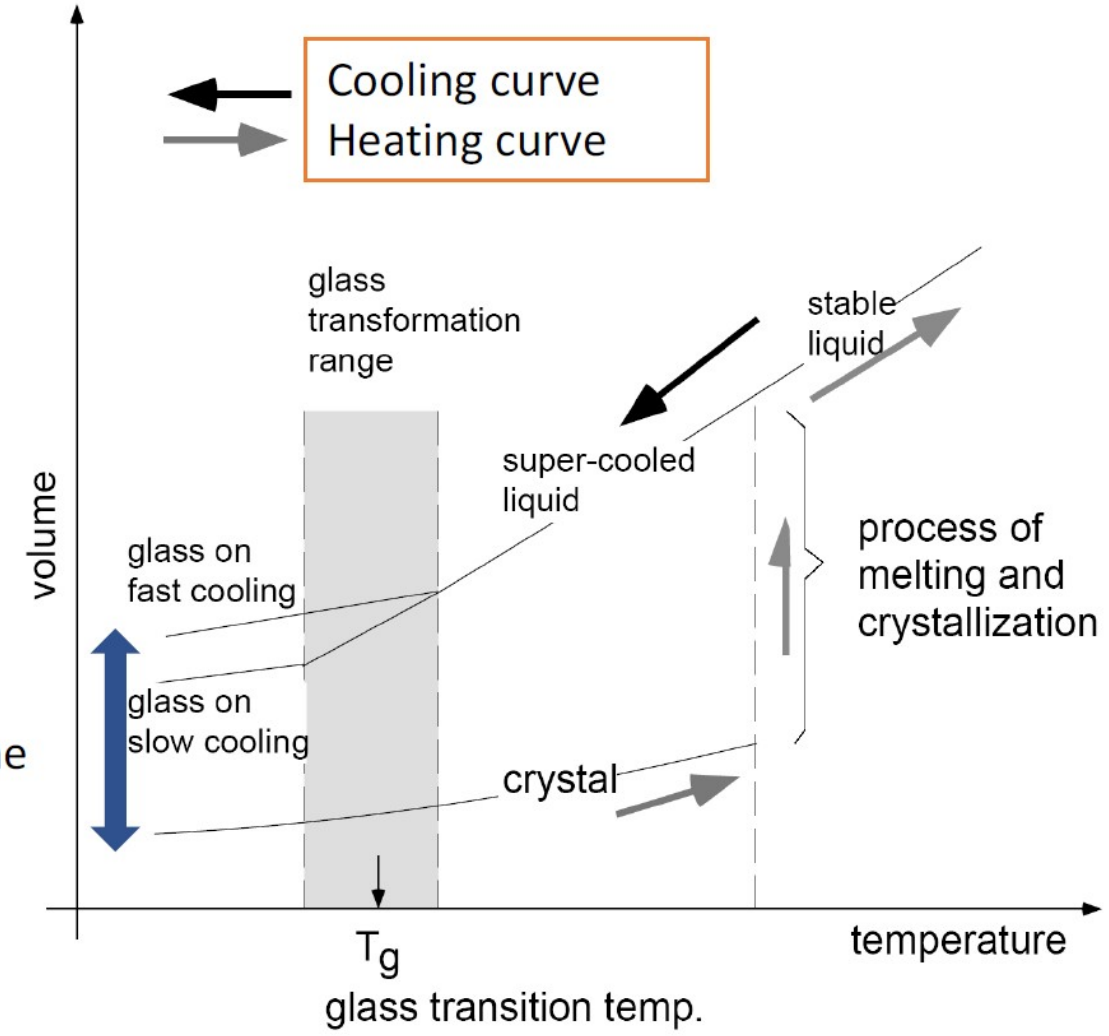

Tg depends on

- atom mobility
- complexity of crystal structure
- cooling rate
- composition

Heating through Tg leads to

- Break down of Van Der Waals Forces
- Onset of large-scale molecular motion
- Polymer goes from glassy/rigid to rubbery behavior
- Upper service temperature in amorphous polymers

Thermodynamics measures: Excess volume

- Energetics of bond density
- Ordered crystal has higher packing -> more bonds per unit volume
- Binding energy $E_{\text{crystal}} < E_{\text{amorphous}}$
- Binding energy <-> molar volume V
- $V_{\text{amorphous}} > V_{\text{crystal}}$
- Excess molar volume $\Delta V = V_{\text{amorphous}} - V_{\text{crystal}}$ is a measure of disorder

Characterization

XRD: amorphous hump

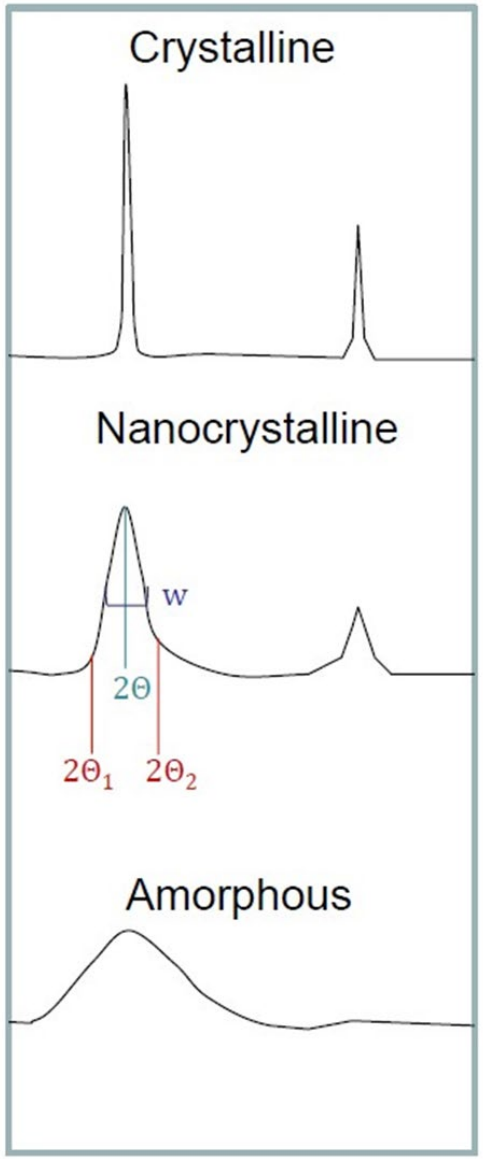

TEM electron diffraction: diffuse ring

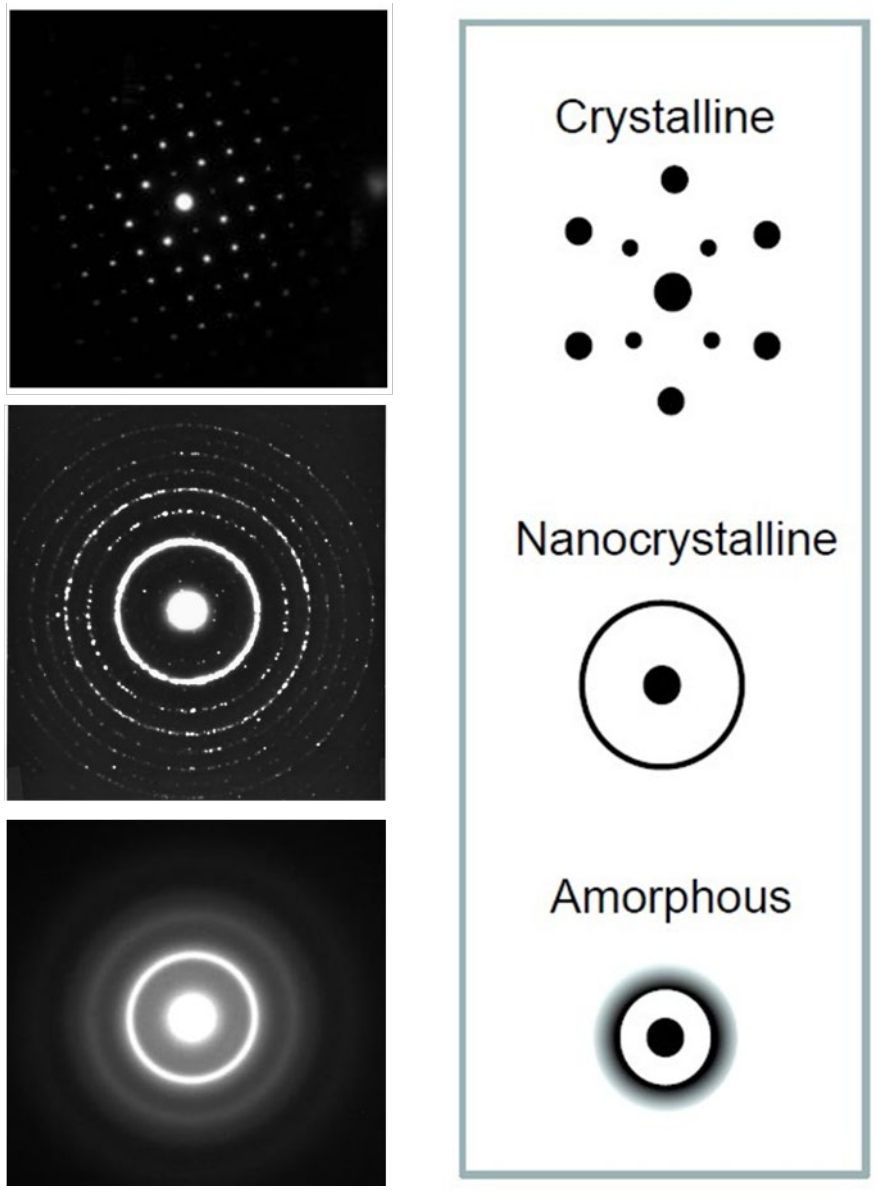

Other methods:

- Spectroscopy (solid state nuclear magnetic resonance, atomic pairwise distribution, infrared spectroscopy, terahertz spectroscopy)
- Extended X-ray Absorption Fine Structure (EXAFS) to probe SRO and MRO: radial distribution function to characterize nearest neighbor arrangements

Methods to generate amorphization

Rapid cooling (quenching) of a melt, low-temperature annealing
Shock waves, femtosecond laser pulses
Mechanical deformation: micropillar compression deformation, high pressure torsion, pressure-induced, static compression or decompression of crystals, tribological load, (prolonged) ball milling, Vickers indentation, tension, static and shock high-pressure experiments, meteorite impact, and deformation by tectonic processes
Focused ion beam
Microwave irradiation, electron beam irradiation, neutron and charged-particle irradiation, pulsed laser irradiation, ion irradiation
Vapor condensation techniques: variations of the method include using an electron beam to vaporize the source or using the plasma-induced decomposition of a molecular species.
Moderate heating
Solid state reactions
Melt spinning
Mechanical alloying
Numerous other methods: lyophilization, spray drying, freeze-drying, dehydration of crystalline hydrates, above the crystallization temperature under an external magnetic field, followed by cooling accompanied with pulse current injection, impregnated in phosphoric acid

First Observation of Shock-Produced Olivine Glass

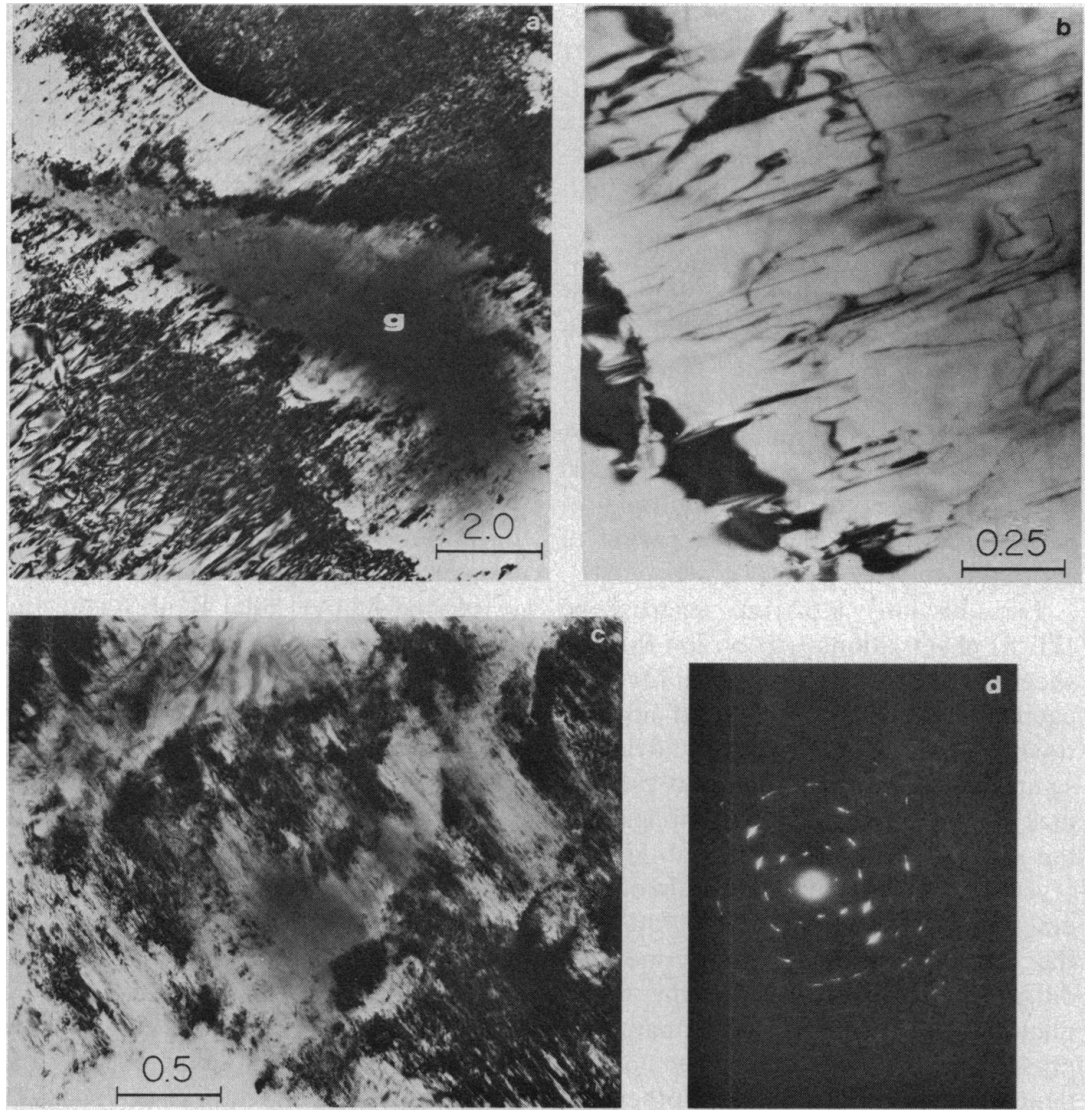

(a) Nondiffracting glassy zone (g) within diffracting and crystalline olivine (light areas) containing a high density of dislocations

(b) Dislocation densities almost as low as in the starting material

(c) Glassy patches (dark, no contrast) grading into crystalline material containing a high density of dislocations.

(d) Electron diffraction pattern of the area in (c)

Exist within crystalline regions with a high density of dislocations at 56 GPa shock pressure

Jeanloz, Science, 1977

Stress-induced amorphization in olivine

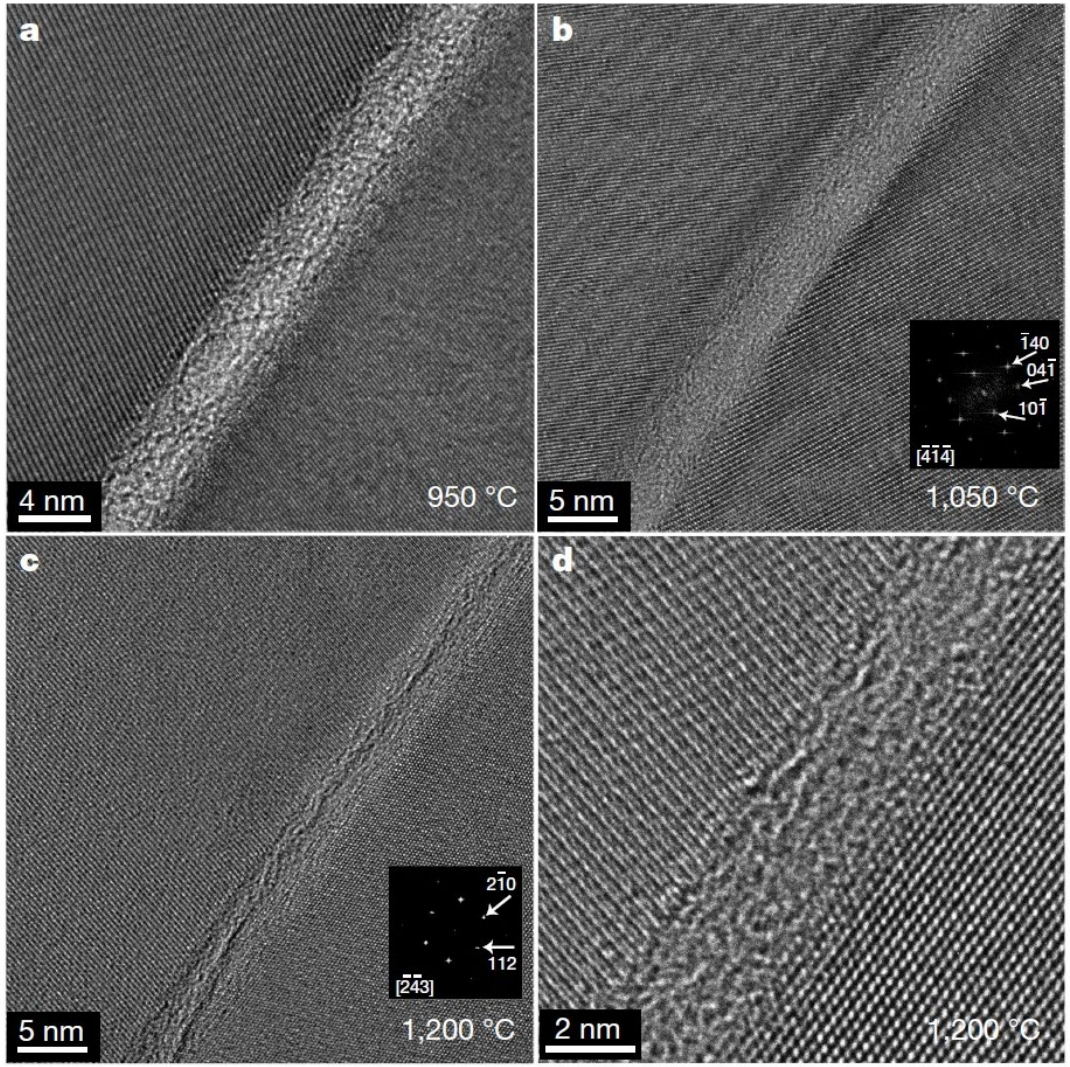

Deformed in the Paterson press at 0.3 GPa

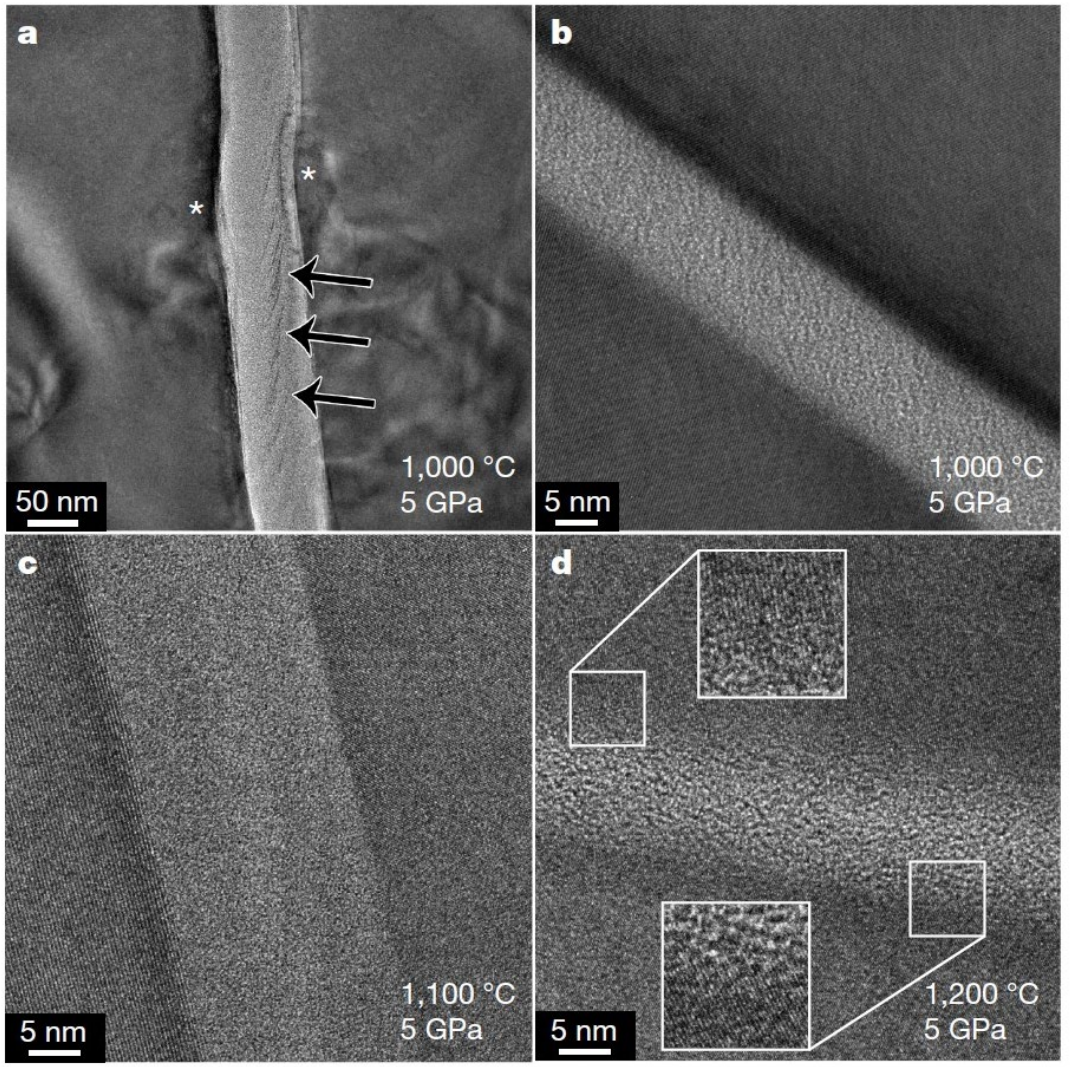

Deformed in the multi-anvil press at 5 GPa

Samae et al, Nature, 2021

AISI 304L stainless steel (Fe–18%Cr–8%Ni)

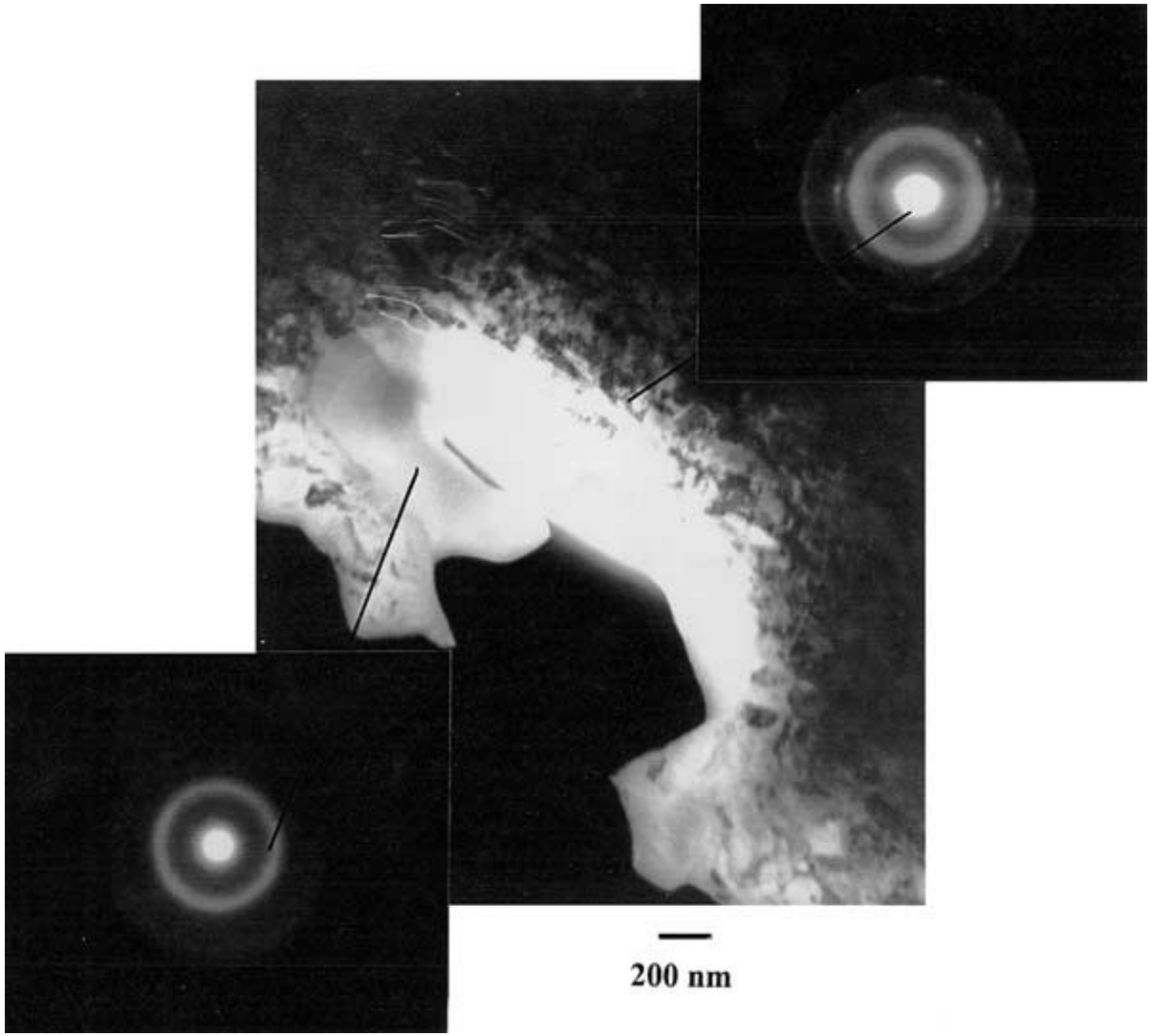

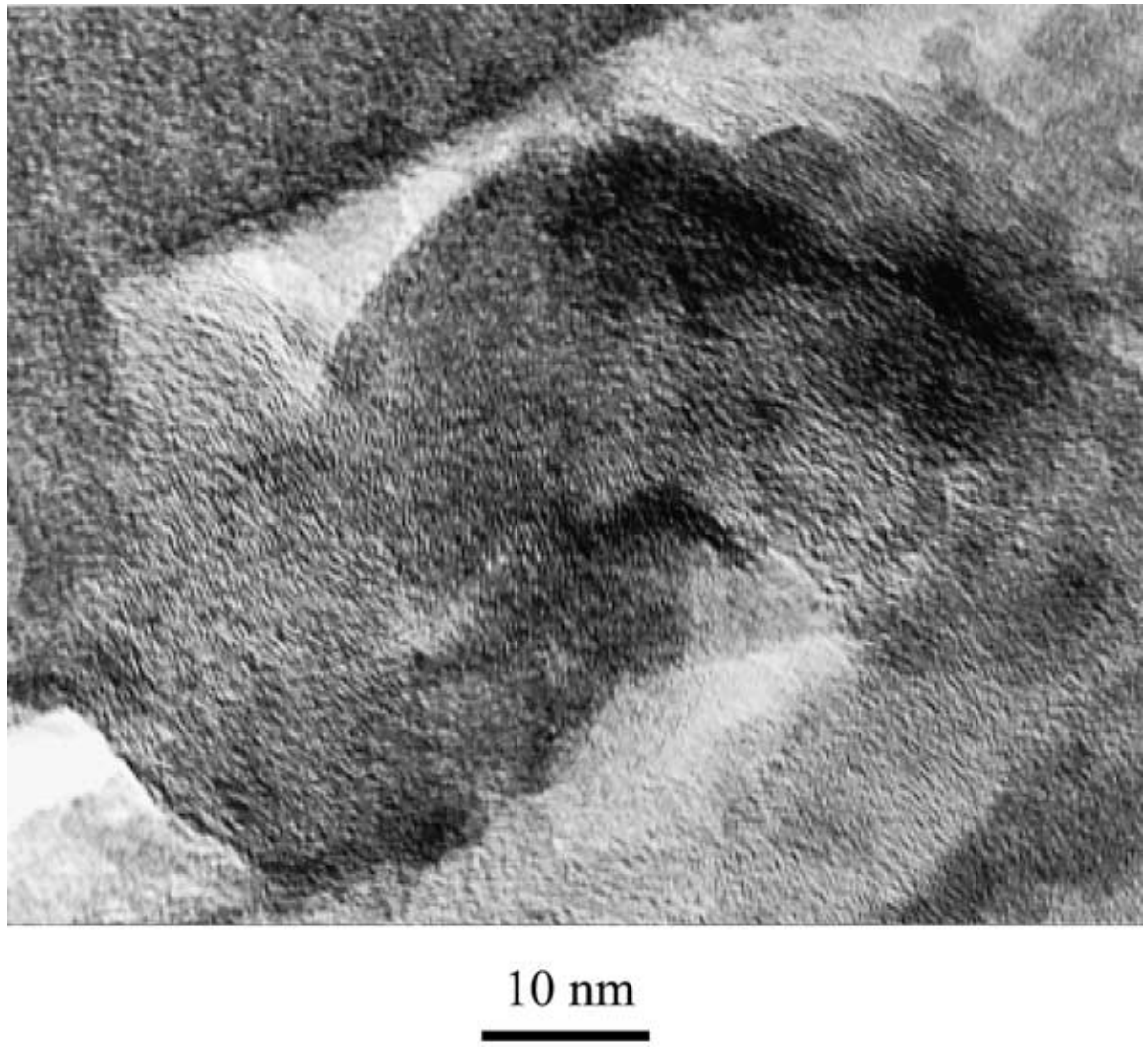

Hat-shaped specimens were deformed in a Hopkinson bar at strain rates of 10^4 s^{-1} and shear strains between 1 and 100.

Meyers et al, Acta Materialia, 2003

High entropy alloy vs. metallic glass

Features	High Entropy Alloys (HEA)	Metallic Glasses (MG)	HE-MG
Number of elements	5 or more	3 or more	5 or more
Ratio of elements	Equal or near-equal atomic percent	One single principal element such as Zr, Cu, Ce, and Fe	Equal or near-equal atomic percent
Configurational entropy	High	Low	High
Number of phases	Single	Single	Single or multiple
Microstructure	Crystalline	Amorphous	Amorphous matrix and crystalline nanoparticles

Yang et al, Acta Metallurgica Sinica (English Letters), 2020

Wang et al, JOM, 2014

HEA and coating

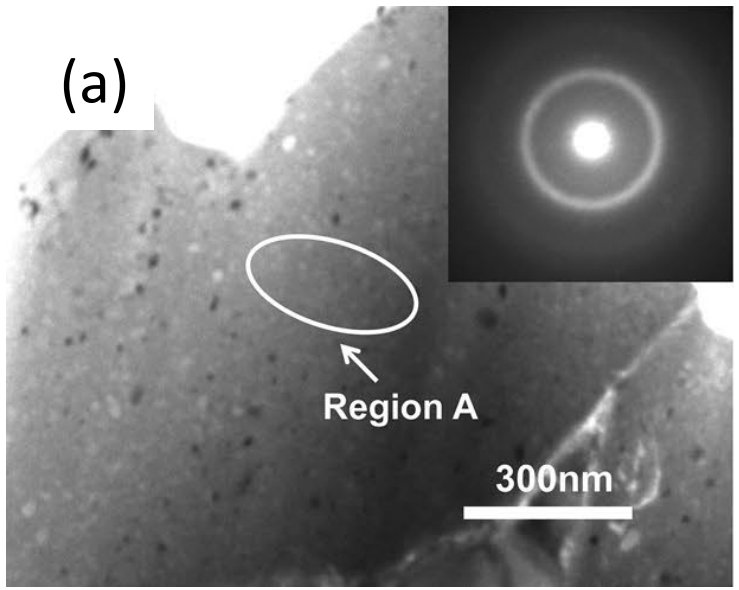

FeCrAlCuNiSi HEA

(a) Amorphous powder molding via a mechanical alloying and ultrahigh pressure consolidation technique.

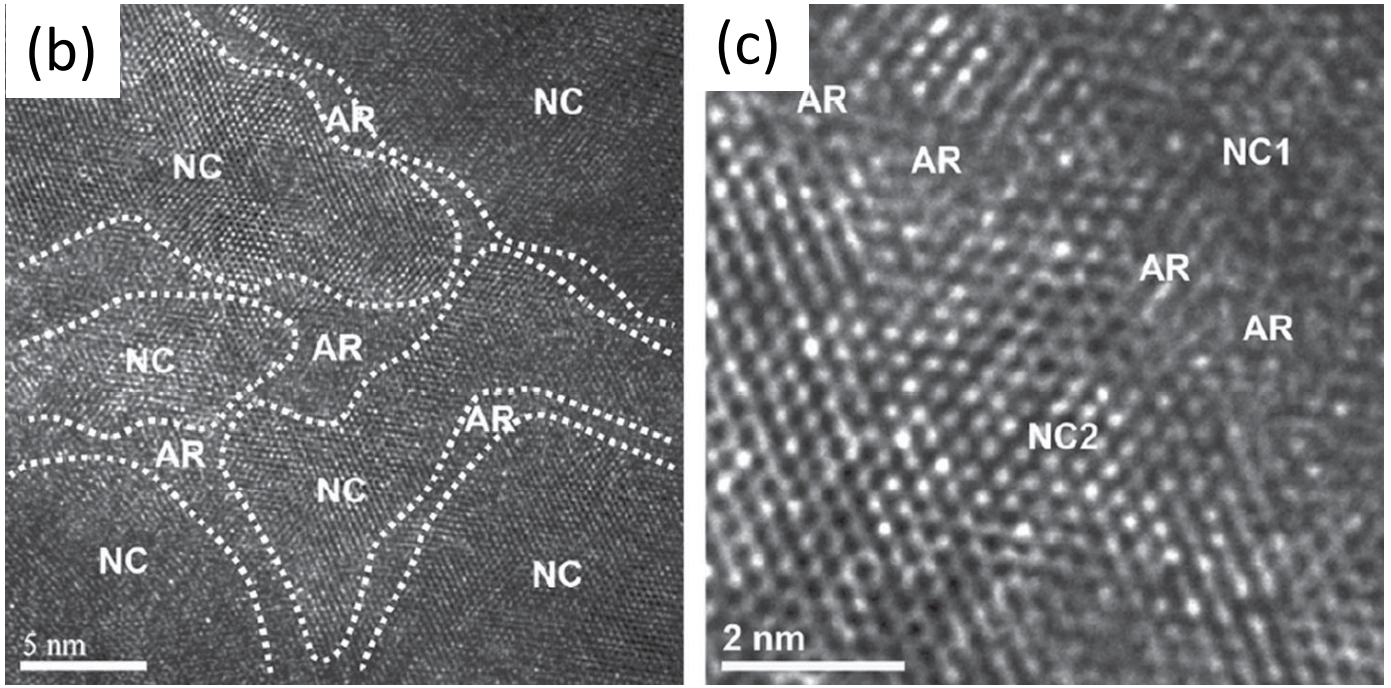

$(AlCrTaTiZr)N_{1.07}Si_{0.15}$ coating

Produced by the reactive RF magnetron sputtering

NC: nanocrystalline, AR: amorphous regions

(c) Magnified image of (b), showing ARs between NC1 and NC2 of small-angle misorientation

Yang et al, Acta Metallurgica Sinica (English Letters), 2020

Li et al, Materials Research Letters, 2018

HEA thin films and coatings

	HEA film or coating (N at.% = 0)			HEA-nitride film or coating			
Composition	Structure	Hardness (GPa)	Elastic modulus (GPa)	Structure at the maximal mechanical properties	Maximal hardness (GPa)	Maximal elastic modulus (GPa)	Preparation method
(AlCrMoTaTiZr)N	Amorphous	11.2	193	FCC	40.2	420	Magnetron sputtering
(AlCrNbSiTiV)N	Amorphous	10.4	177	FCC	41	360	Unbalanced magnetron sputtering
(AlCrSiTiZr)N	Amorphous	11.5	–	FCC + Amorphous	19.6	227.5	Magnetron sputtering
(NbTiAlSiW)N	–	–	–	Amorphous	13.6	154	Magnetron sputtering
(TiHfZrVNb)N	–	–	–	FCC	44.3	384	Cathodic arc vapor
(TiVCrAlZr)N	Amorphous	8.2	128.9	FCC	11	151	Magnetron sputtering
(AlCrTaTiZr)N	Amorphous	9.3	140	FCC	32	368	Magnetron sputtering
(TiVCrZrHf)N	Amorphous	8.3 ± 1.3	104.7 ± 3.1	FCC	23.8 ± 0.8	267.3 ± 4.0	Magnetron sputtering
(AlCrMnMoNiZr)N	Amorphous	7.2	172	FCC	11.9	202	Magnetron sputtering
(FeCoNiCuVZrAl)N	Amorphous	8.6	153	Amorphous	12	166	Magnetron sputtering
(AlBCrSiTi)N	Amorphous	–	–	Amorphous	23	256.6	Magnetron sputtering
(ZrTaNbTiW)N	Amorphous	4.7	120.0	FCC + BCC	13.5	178.9	Magnetron sputtering + PBII
(FeCoNiCrCuAlMn)N	FCC + BCC	4.2	–	Amorphous	11.8	–	Magnetron sputtering
(FeCoNiCrCu$Al_{0.5}$)N	FCC	4.4	–	Amorphous	10.4	–	Magnetron sputtering
(AlCrTaTiZr)N	Amorphous	–	–	FCC	35.2	–	Magnetron sputtering
(AlCrNbSiTi)N	–	–	–	FCC	36.7	–	Magnetron sputtering
(AlCrTaTiZr)N	–	–	–	FCC	36	360	Magnetron sputtering
(AlCrTaTiZr)N	–	–	–	FCC	35	350	Magnetron sputtering
(TiZrNbHfTa)N	FCC + compounds	5.4 ± 0	–	FCC	32.9 ± 1	–	Magnetron sputtering
(TiVZrNbHf)N	BCC	8.1	–	FCC	66.0	–	Vacuum arc deposition
(AlCrTaTiZrSi)N	–	–	–	FCC	30.2	258	Magnetron sputtering

Nanocrystalline nickel

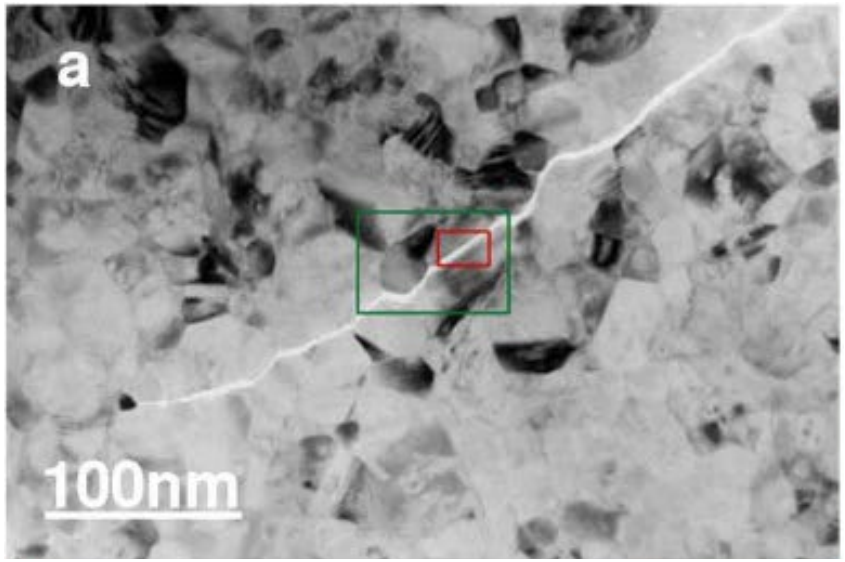

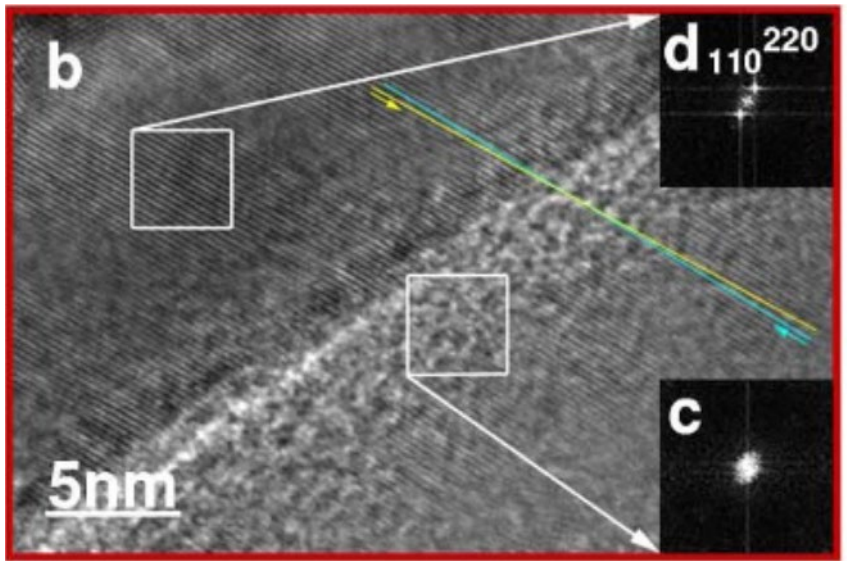

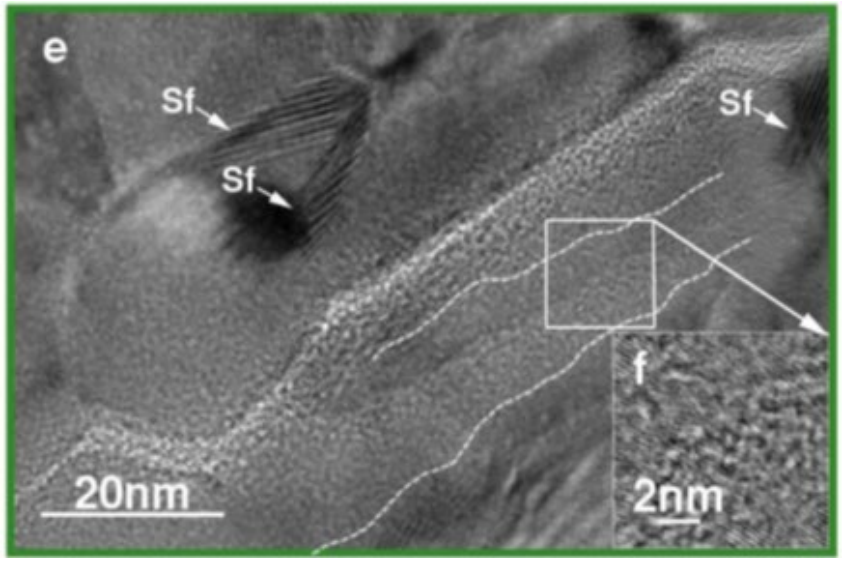

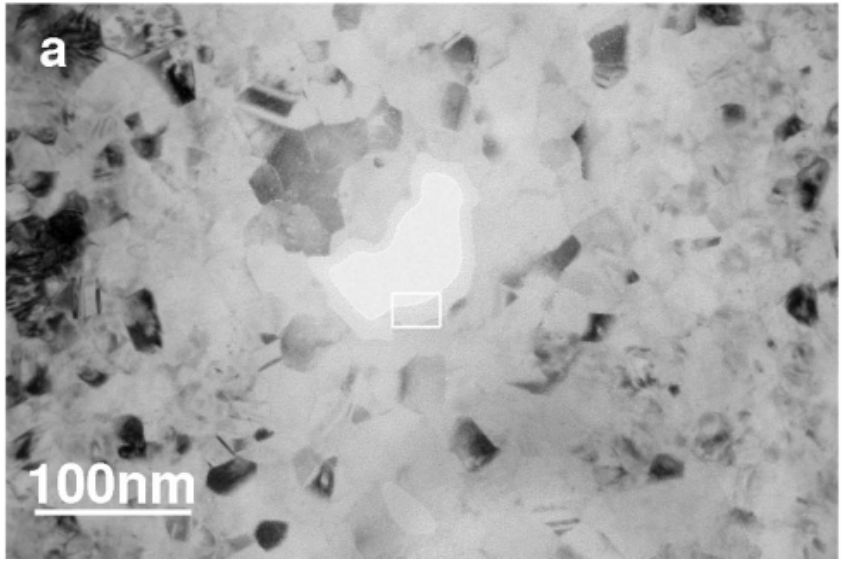

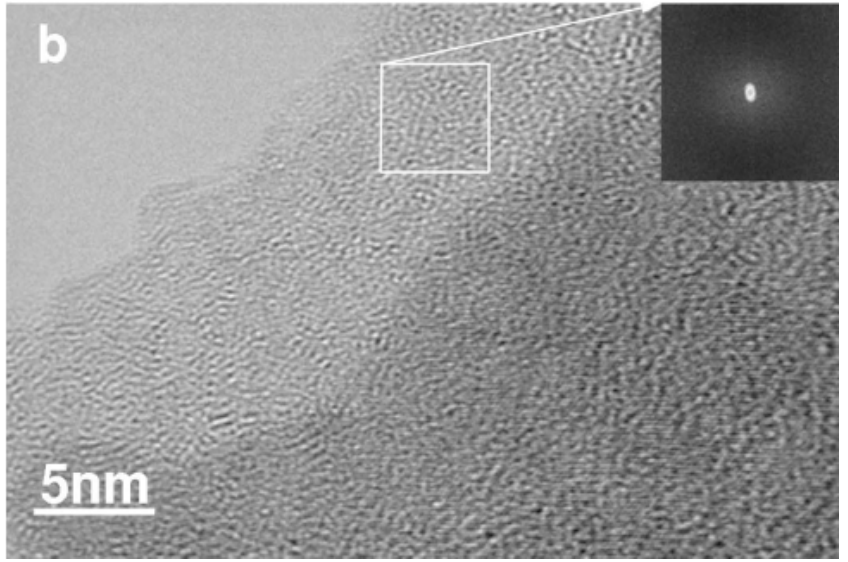

Deformed by quasi-static compression at a strain rate of 10^{-5} s^{-1}

Han et al., *Scientific Reports,* 2012

Intermetallic ($SmCo_5$)

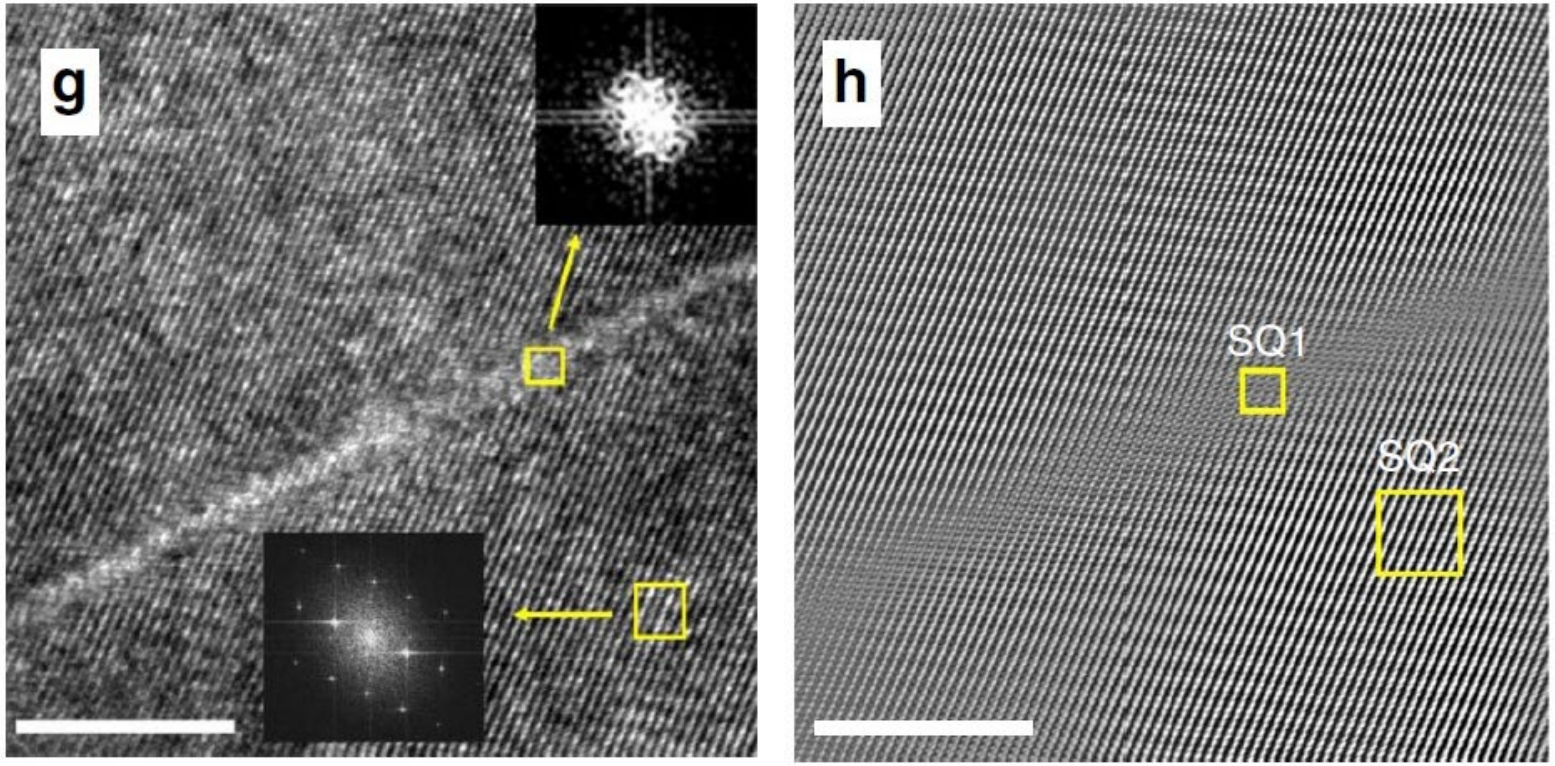

Nanoindentation deformed maximum loading 6000 μN, dwelling step 10 s and the nanoindentation size ~700 nm

g. The HRTEM image of a selected shear band and its surrounding regions. FFT patterns are in the insets. Scale bar: 10 nm
h. The inverse FFT image shows a blurred stripe corresponding to the amorphous shear band while the off-band regions are crystalline

Luo, Szlufarska, *et al., Nature Communications*, 2019
Luo, Szlufarska, et al., Materials Science and Engineering A, 2020

Ni and Si Nanowires

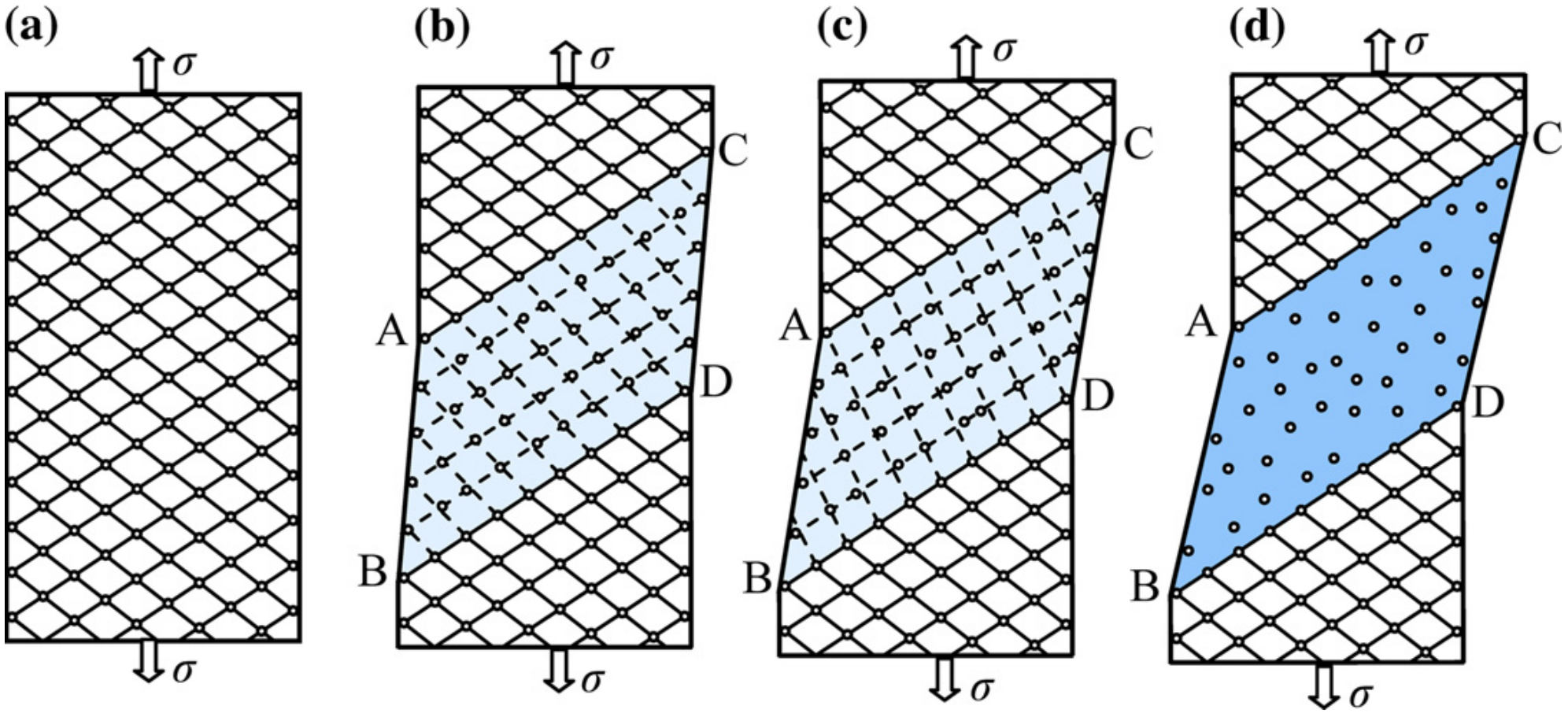

Single crystalline nanowire under uniaxial tensile load along its axis

Ovid'ko, Scripta Materialia, 2012

Covalent materials

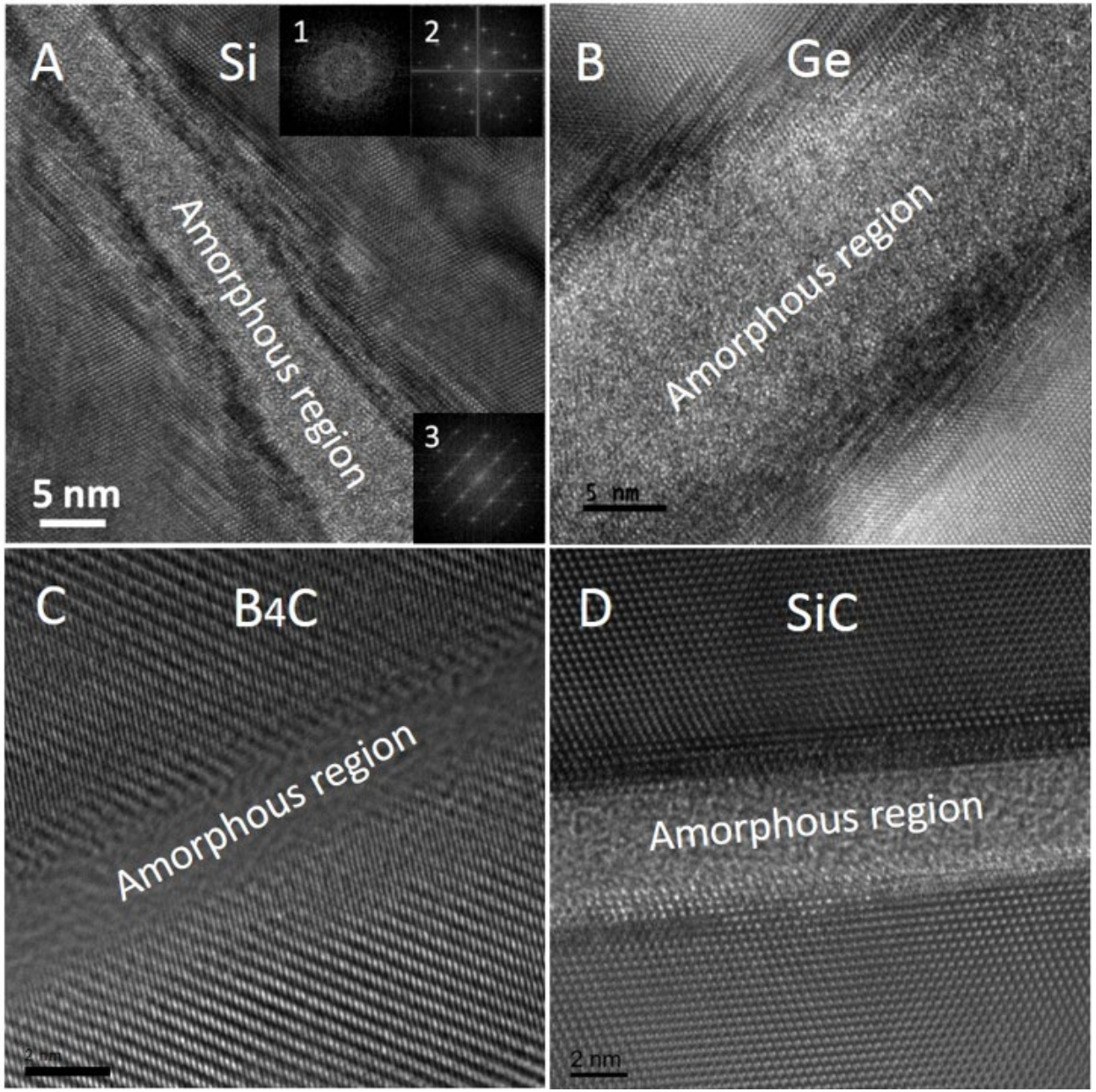

Shocked by high energy laser pulse

Material	Experimental shock stress (GPa)
Si	20
Ge	10
B_4C	50
SiC	45

Zhao *et al.,* DYMAT, 2018

Amorphization as a deformation mechanism under extreme conditions

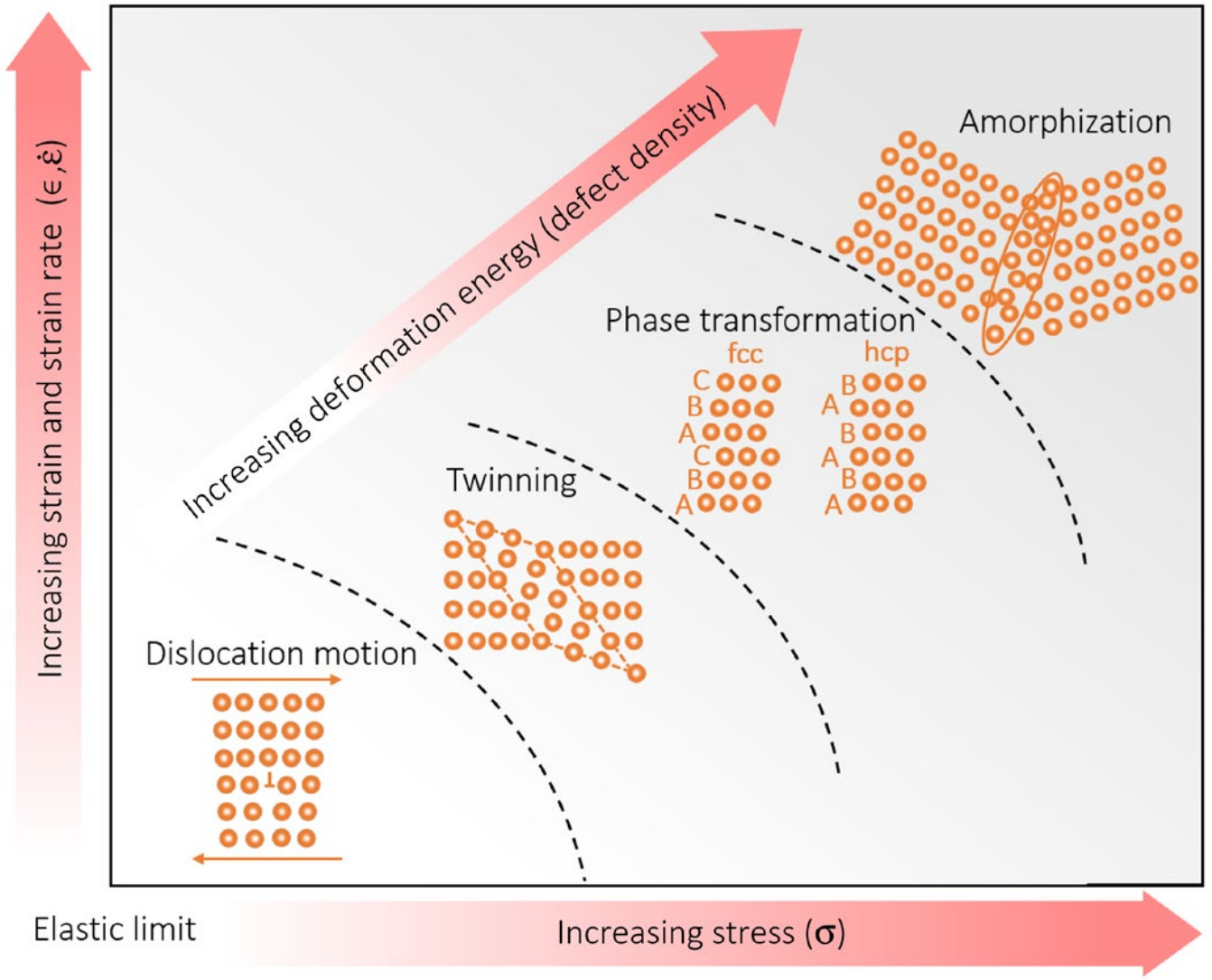

As stress increases, strain rate and temperature lead to four different shear-driven deformation mechanisms.

Zhao et al., Sci. Adv. 2021

Shock + Shear Induced Amorphization

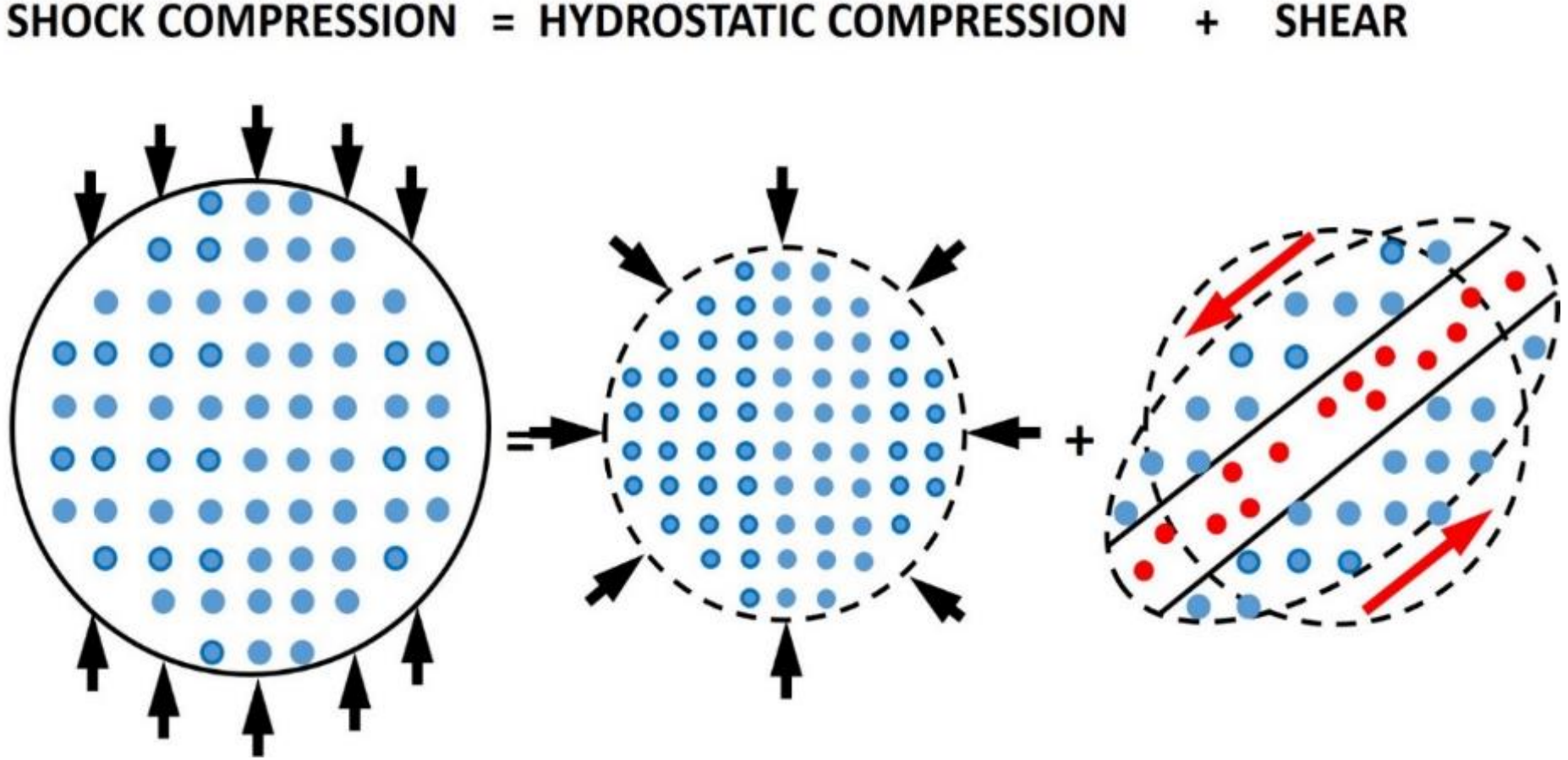

Zhao et al., 2019

Reversibility, partial irreversibility, and irreversibility of glass under simple shear

Deformation cycle: (0, 0)→(ϵ, 0)→(ϵ, γ)→(ϵ, 0)

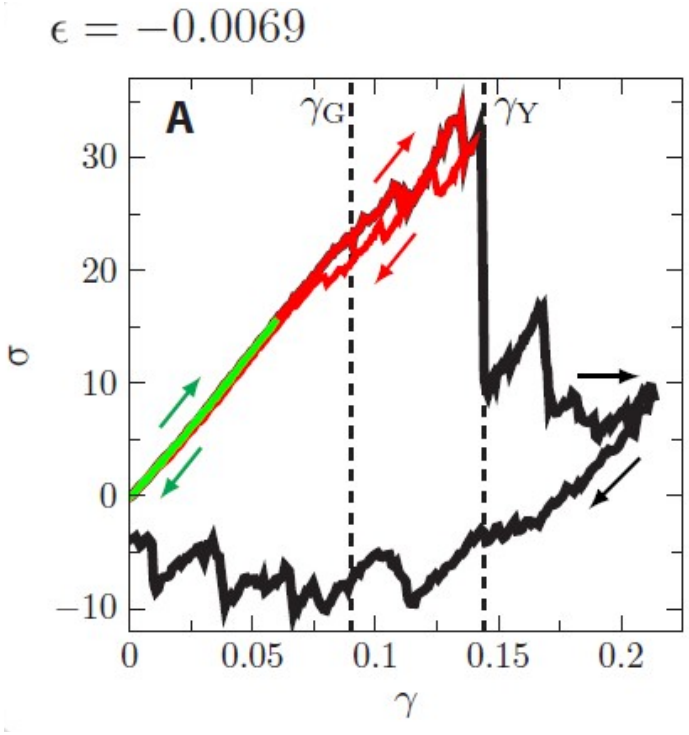

Fig. 1 At the yielding strain γ_Y, a sudden and notable stress drop occurs, the entire system fractures and breaks, yielding is irreversible.

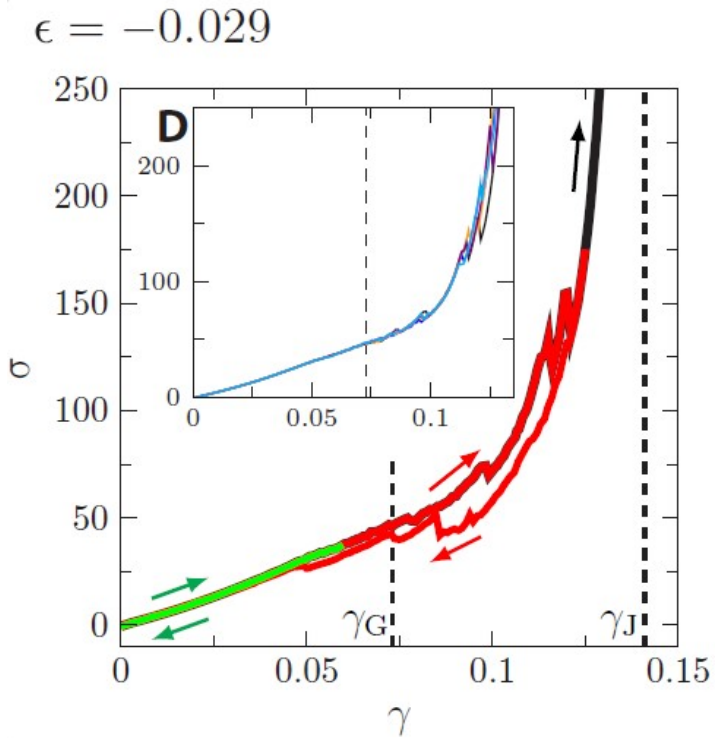

Fig. 2 The system is compressed more before shearing. It jams at the shear jamming strain γ_J by the divergence of the shear stress.

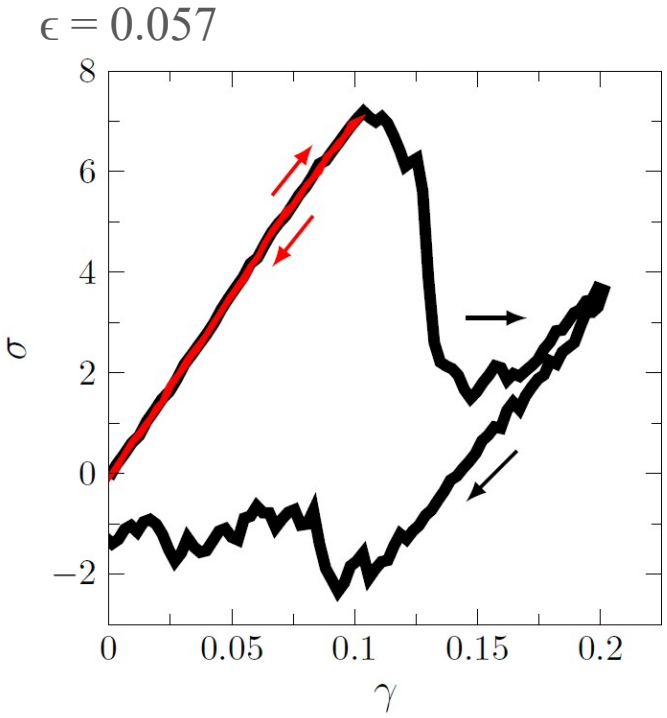

Fig. 3 The system does not go through the partially irreversible regime under shear up to the yielding.

Jin et al., Sci. Adv. 2018

Amorphous solids: elastic or plastic

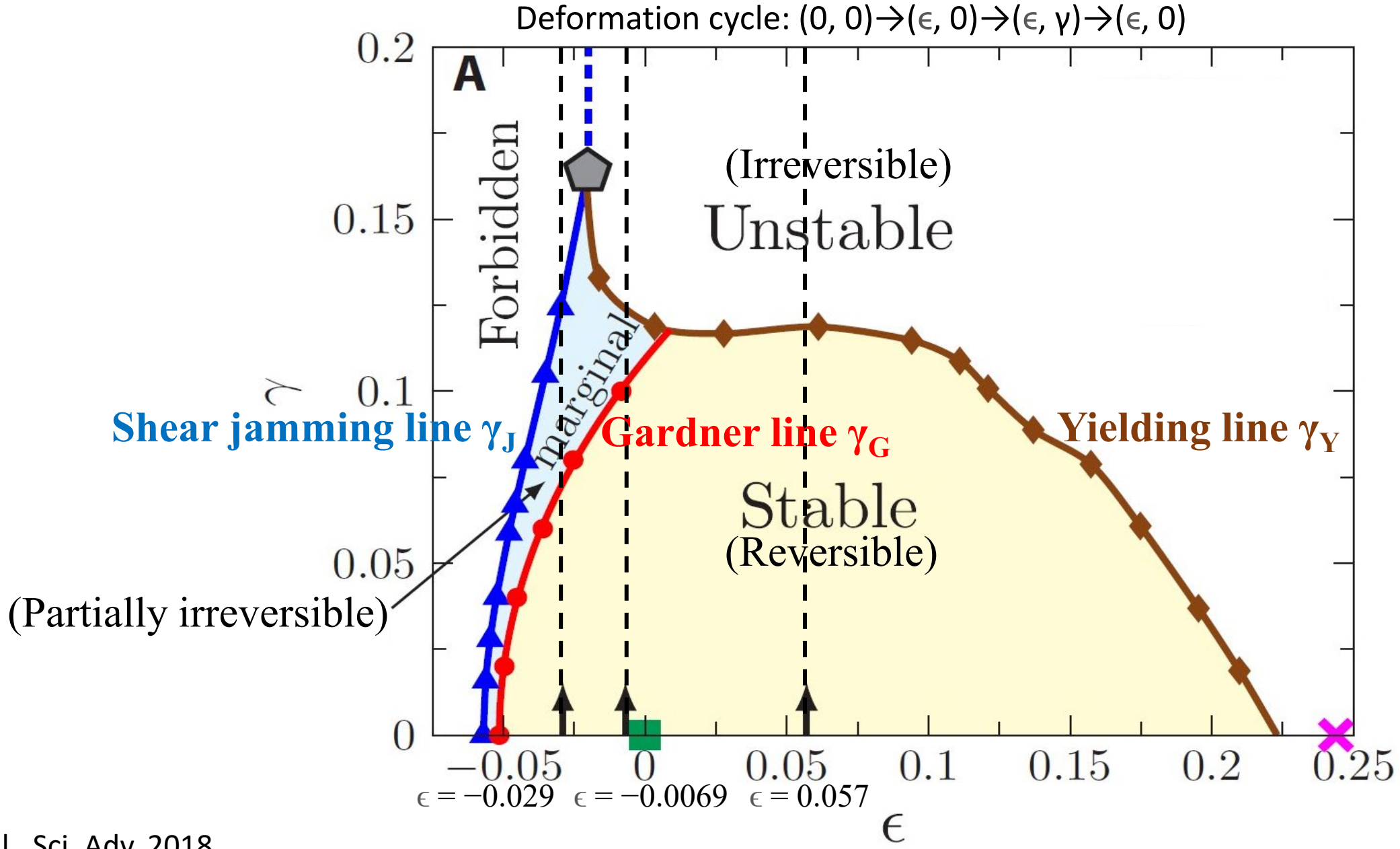

Jin et al., Sci. Adv. 2018

Free Volume

• The free volume is the empty space in a solid or liquid that is not occupied by molecules.

• Free volume is high in liquid state than solid, so molecular motion can take place relatively easy because the unoccupied volume allows the molecules to move.

• The theory was originally developed for amorphous polymers and the glass-transition in those polymers.

• An amorphous polymer can be made up of occupied volume and free volume. As the temperature is changed, the free volume and the occupied volume both will change.

• Free volume in amorphous materials may be considered as a carrier of plasticity equivalent to dislocations in crystalline materials.

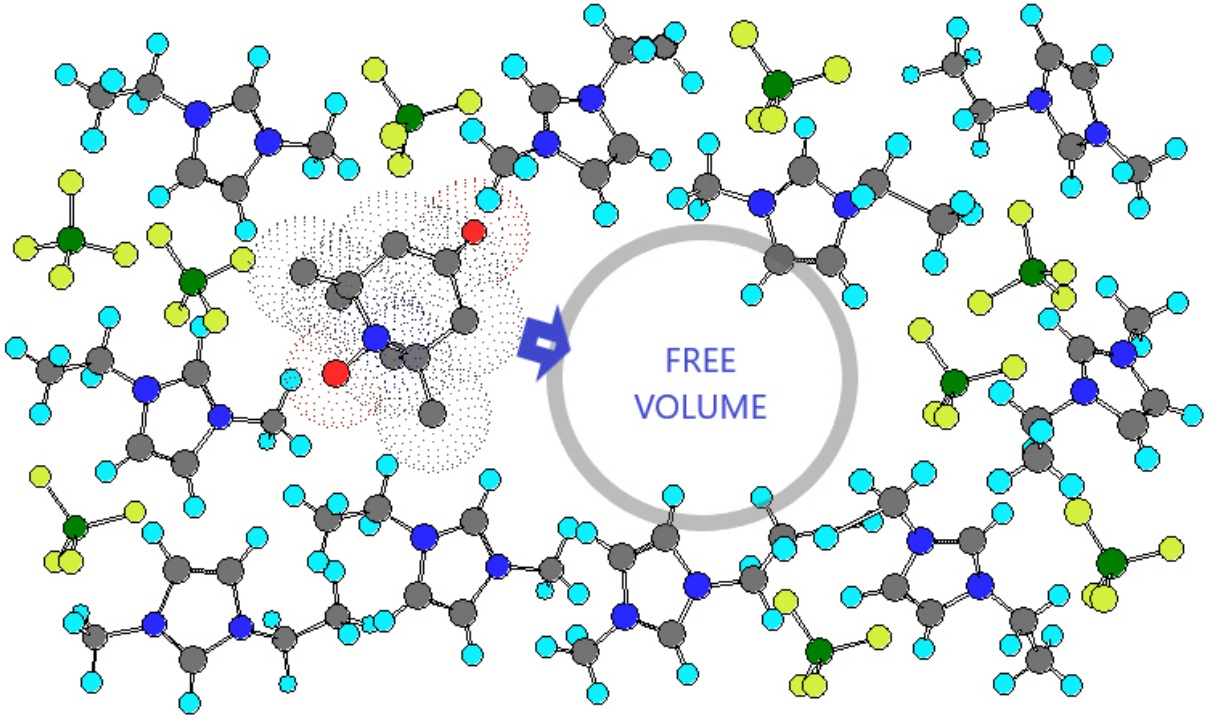

Free Volume Theory

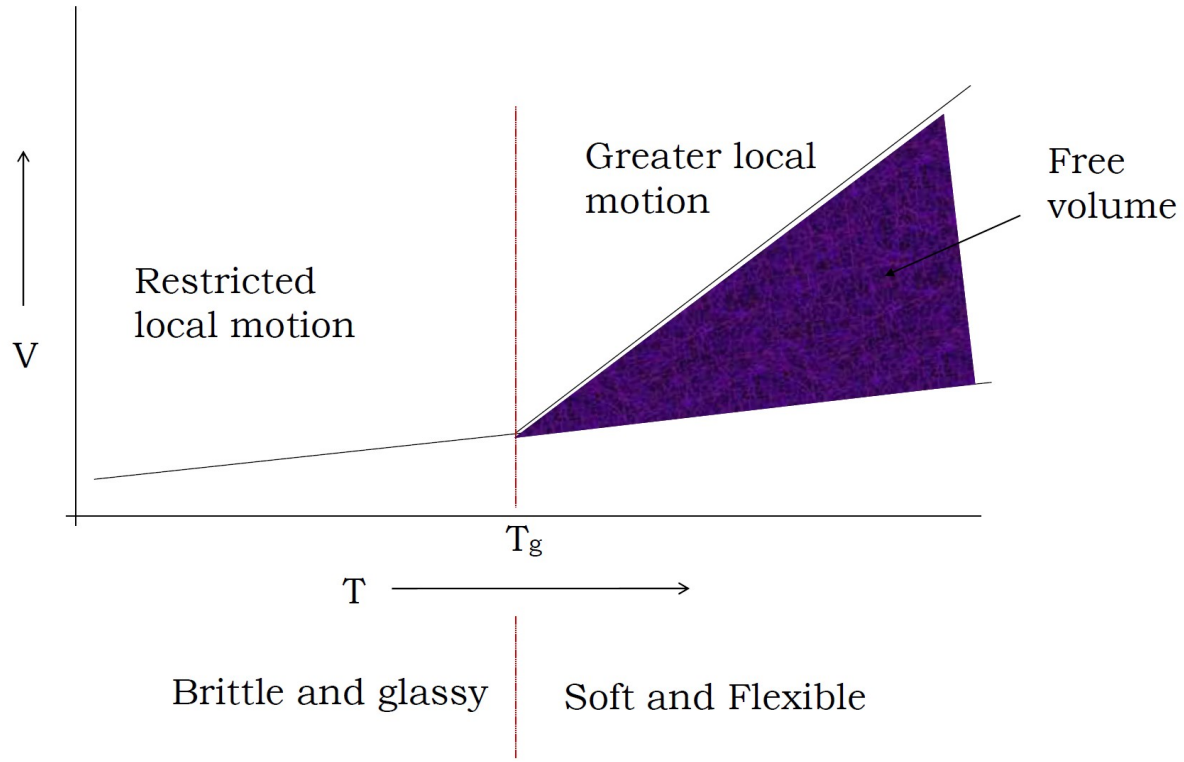

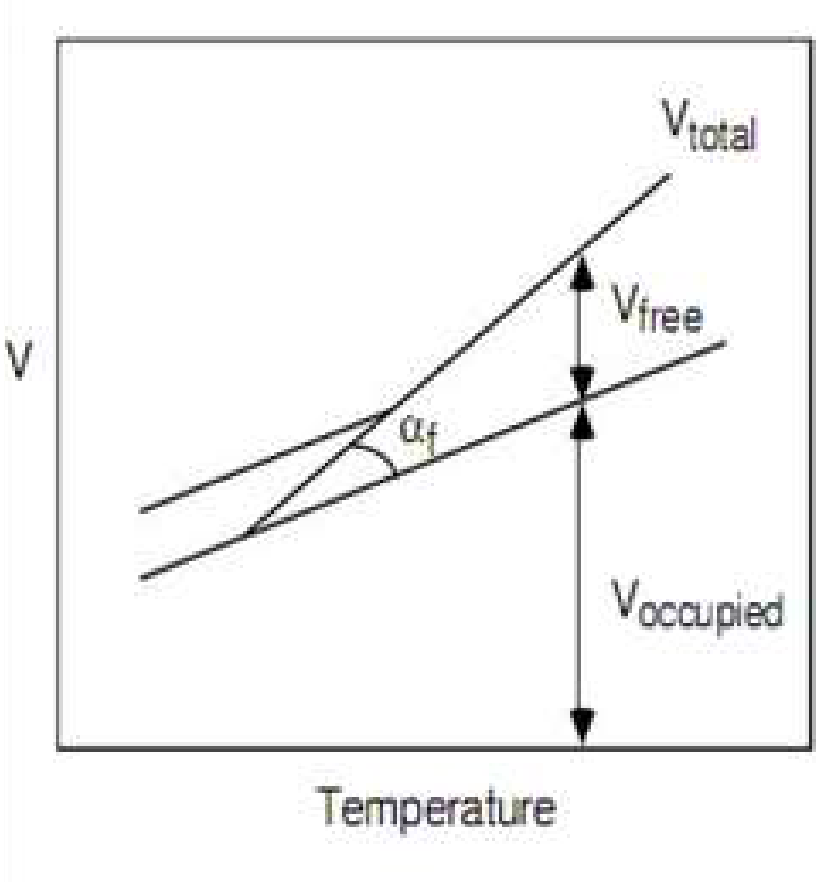

As the temperature of the melt is lowered, the free volume will be reduced until eventually there will not be enough free volume to allow molecular motion or transition to take place.

The free volume of BMGs is a part of the volume and changes with temperature, i.e., the free volume being released out in structural relaxation and reproduced in glass transition.

Shear transformation zone (STZ) dynamics model

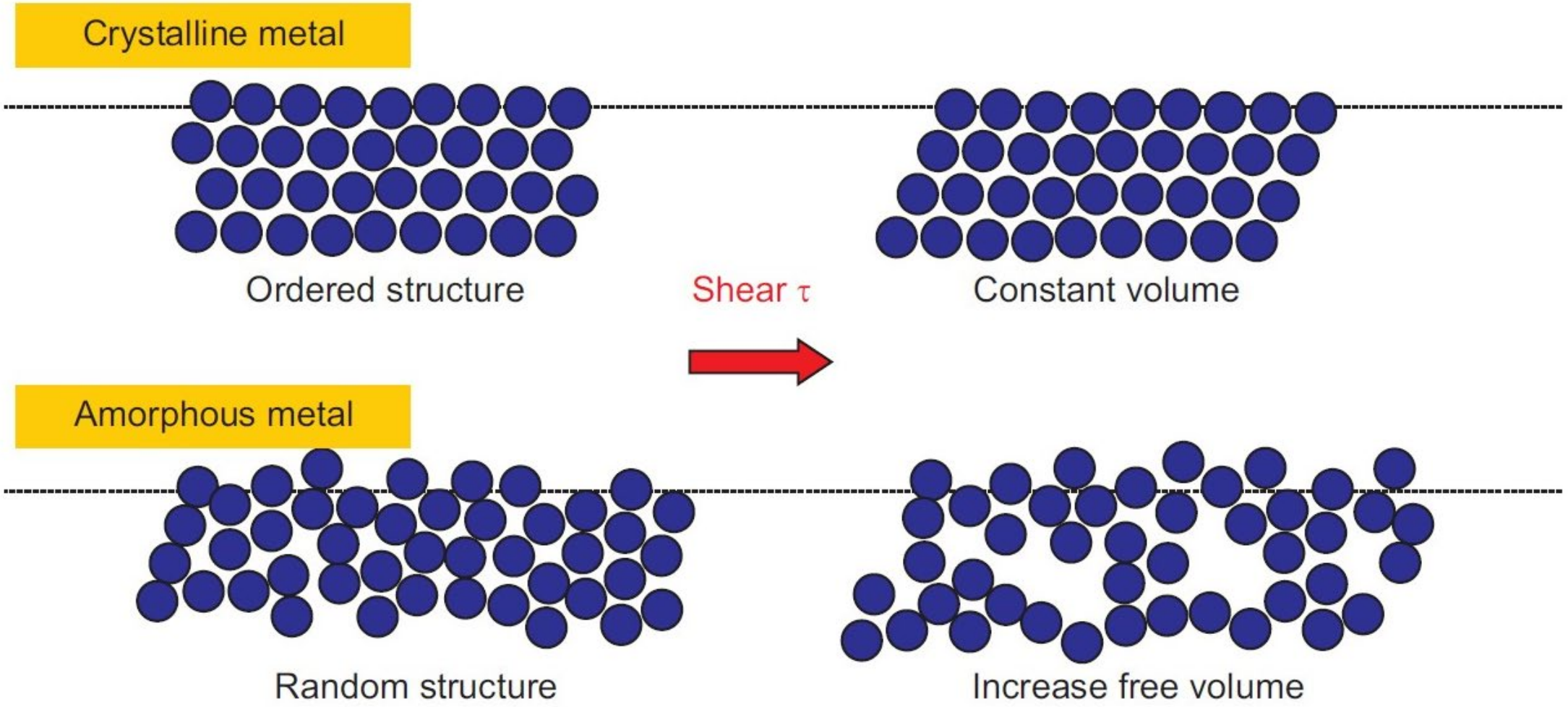

Atomic structures of crystalline and amorphous metal

Park, Appl Microsc, 2015

Dislocations versus Shear bands

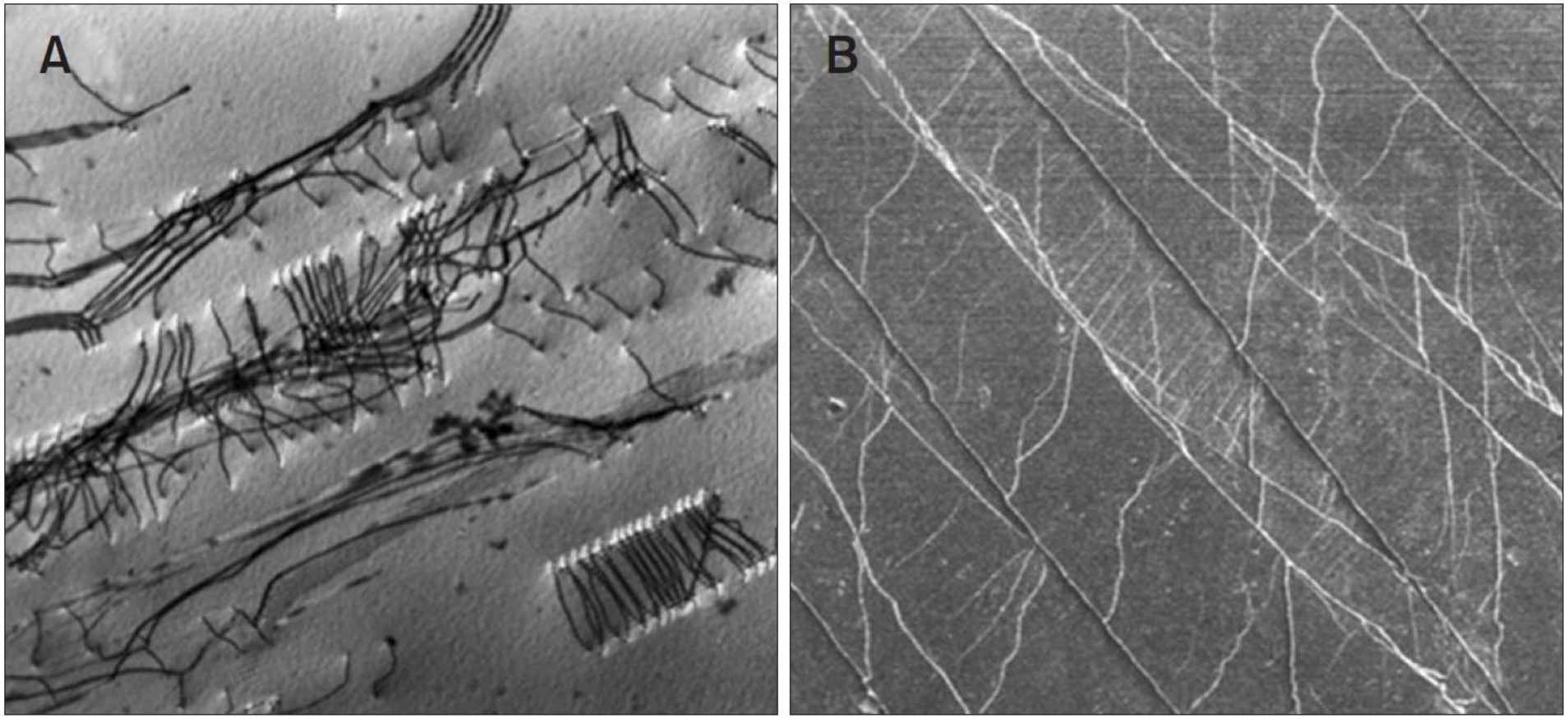

(A) TEM image of deformed 316 stainless steel showing dislocations and dipoles on (111) planes
(B) SEM image of deformed BMG showing multiple shear bands on the surface of the sample

Park, Appl Microsc, 2015

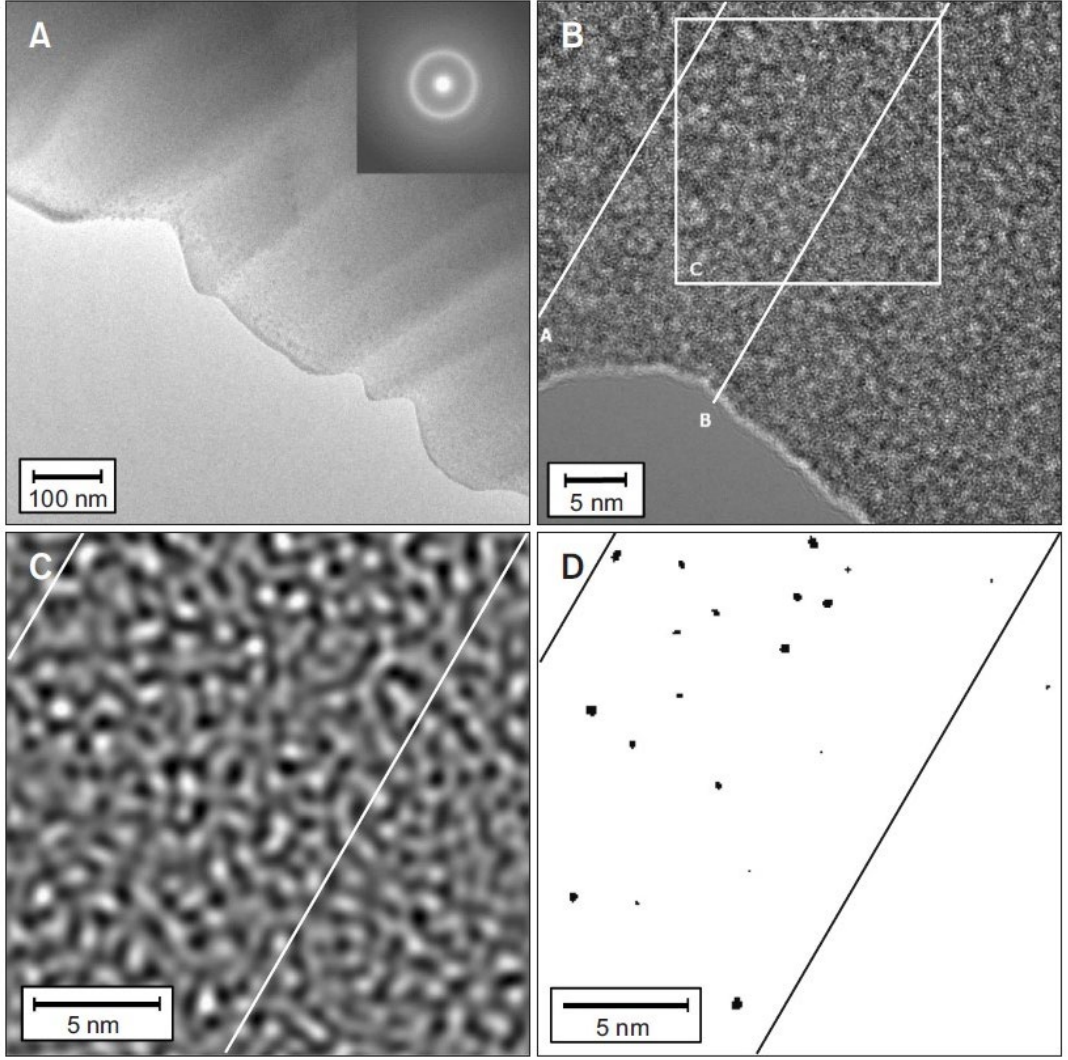

(A) Low magnification and (B) high resolution TEM micrograph taken from the widely spaced shear band area produced by bending an amorphous metal. (C) Fourier filtered image (D) the black spots correspond to bright features in Fig. C (regions of excess free volume).

In Fig. B-D, free volume has accumulated preferentially in the shear band, nanoscale voids of ~1 nm size and less are observed within the shear band in Fig. D.

Park, Appl Microsc, 2015

Shear transformation zone (STZ) theory

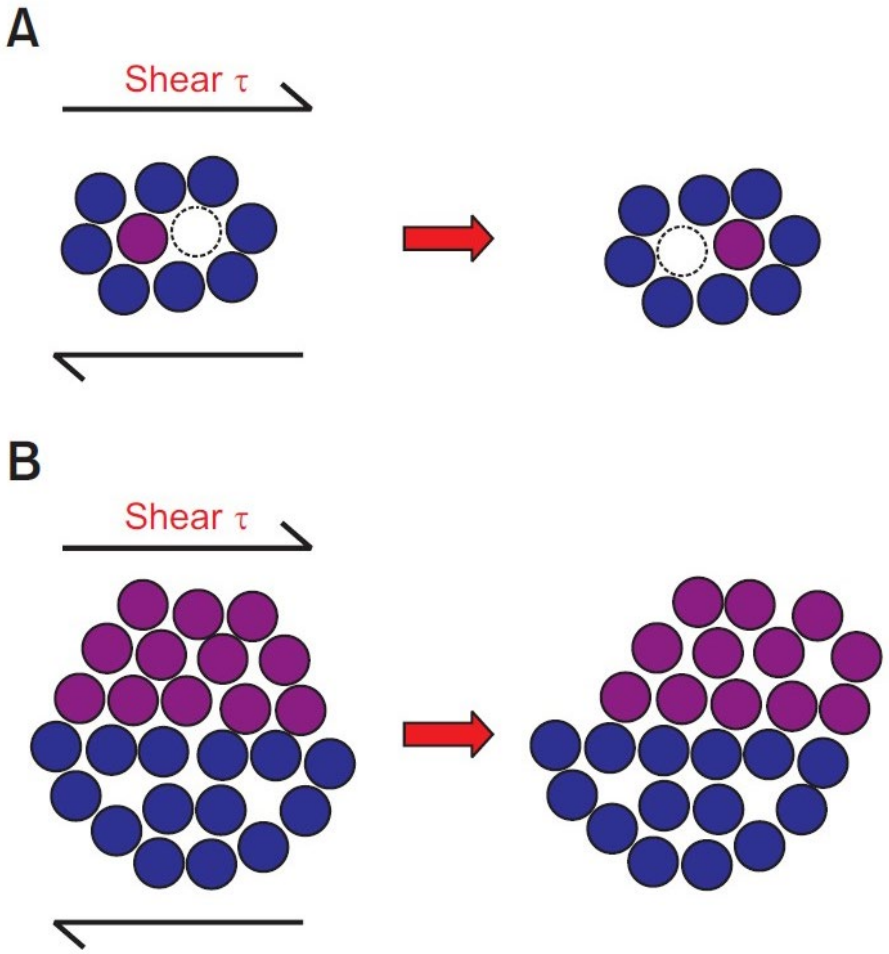

Two-dimensional schematic diagram of the atomistic deformation mechanisms proposed for amorphous metals, including an individual atomic jump (macroscopic diffusion and flow) (A, Spaepen [1977]) and a shear transformation zone (spontaneous and cooperative reorganization) (B, Argon [1979]).

Park, Appl Microsc, 2015 Argon, Acta Metall. (1979)

Shear deformation in metallic glass

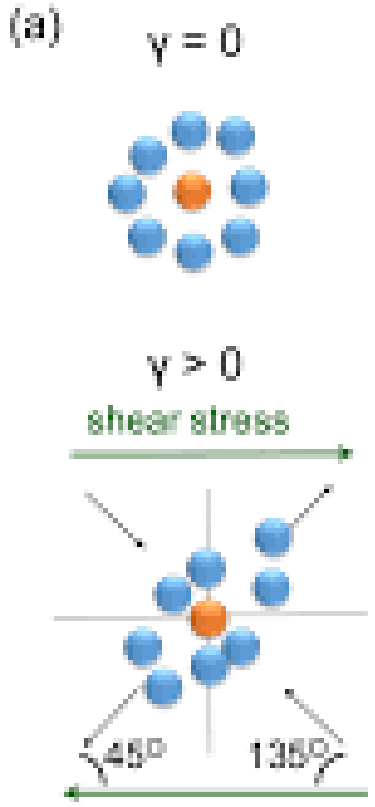

(a) Large nonaffine displacements cause particles in the shear plane to leave the glassy cage outward along the 45◦ line and to be pushed inward towards the center along the 135◦ line leading to local density changes.

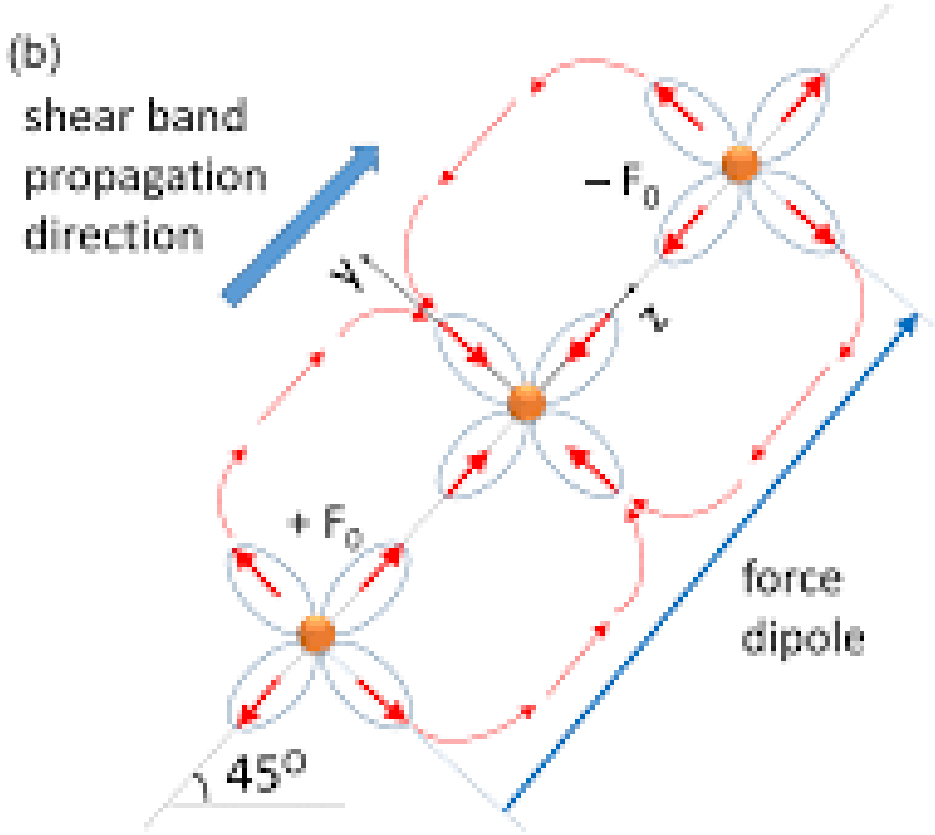

(b) Illustration of the idea that density changes are caused by an alignment of Eshelby-like quadrupoles along the 45° direction.

Hieronymus-Schmidt et al, PHYSICAL REVIEW B, (2017)

Alternating density variations in shear bands

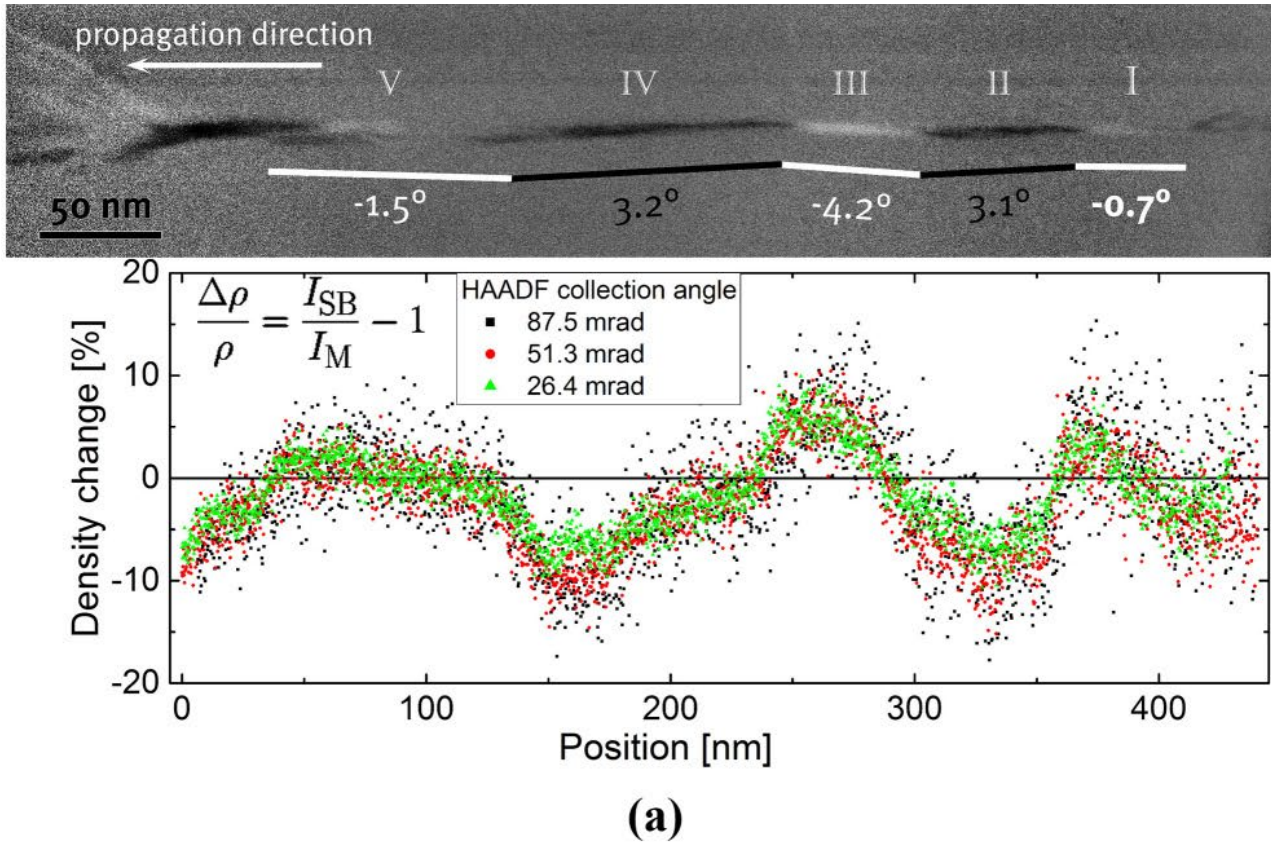

(a)

(a) Top: HAADF-STEM image showing contrast reversals (bright-dark-bright) in a shear band of cold-rolled Al88Y7Fe5 MG. Bottom: Corresponding quantified density oscillations along the shear band for different collection angles of the HAADF detector. Negative amplitudes correspond to dilated regions whereas positive amplitudes refer to densified regions of the shear band compared to the surrounding matrix.

Hieronymus-Schmidt et al, PHYSICAL REVIEW B, (2017)

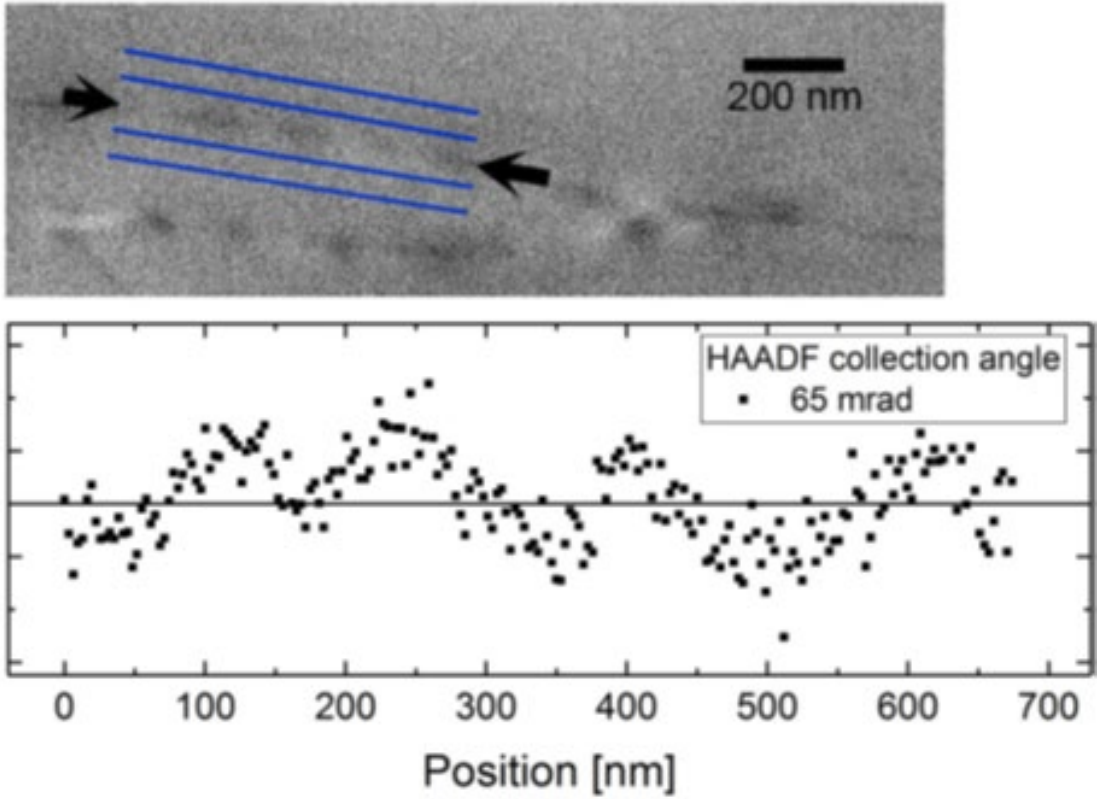

(b)

(b) Top: HAADF-STEM image showing contrast reversals (bright-dark-bright) in a shear band (see arrows) of a compression deformed BMG (Zr52.5Cu17.9Ni14.6Al10Ti5, Vitreloy105). Bottom: Corresponding quantified density oscillations along the shear band.

The mechanical properties of BMGs can be adjusted by the same means for crystalline materials even though the mechanisms are very distinct.

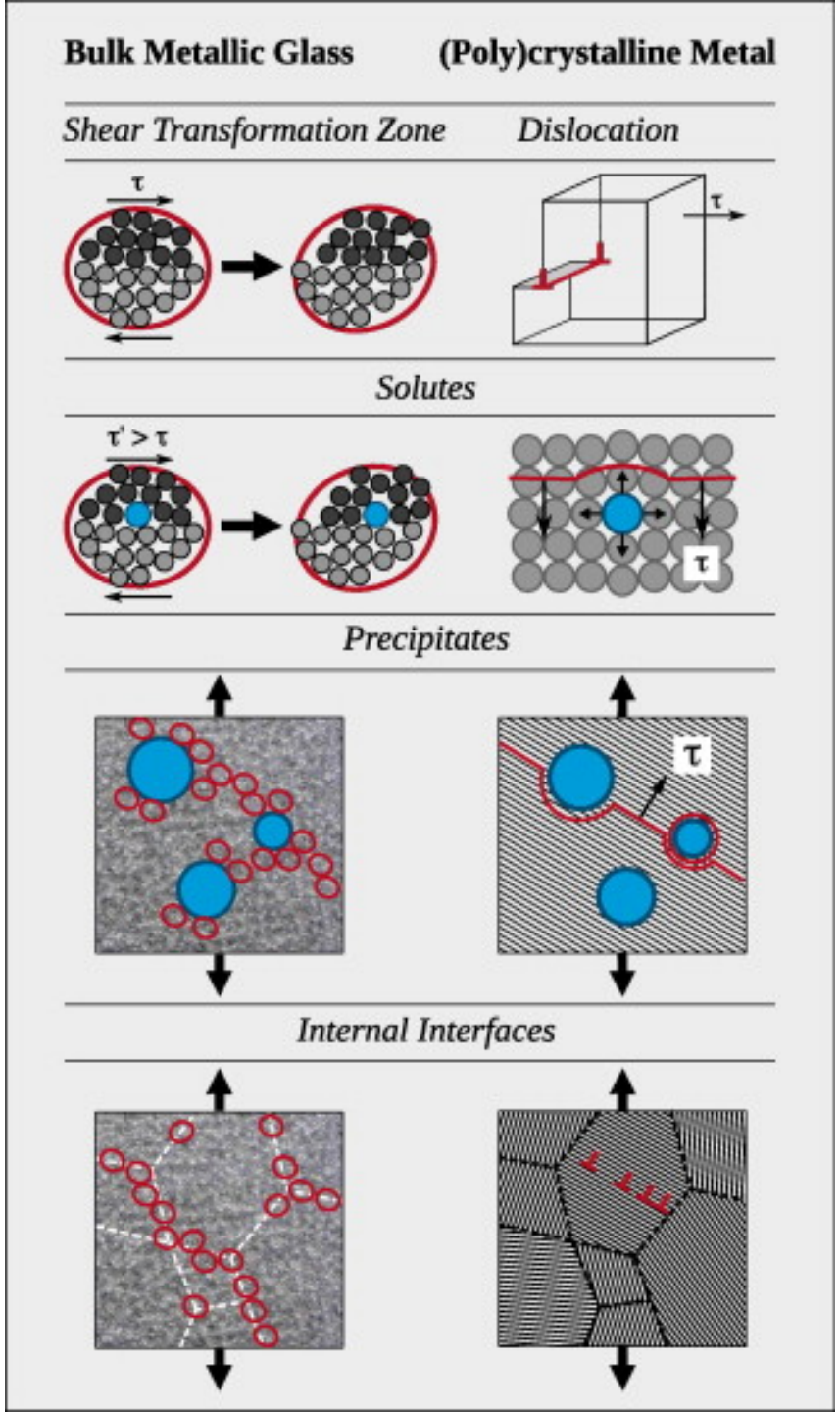

In contrast to crystalline metals, microstructural defects in glasses primarily promote the formation of STZs and shear band nucleation. The formation of multiple shear bands cannot only be induced by secondary phases or nanoprecipitates, but also by interfaces in nanoglasses.

Albe, Mechanics of Materials, 2013

Molecular dynamics simulation

3dp (3D periodic boundary conditions): a homogeneous metallic glass in the absence of stress concentrators

2dp: a sample with free surfaces in one direction

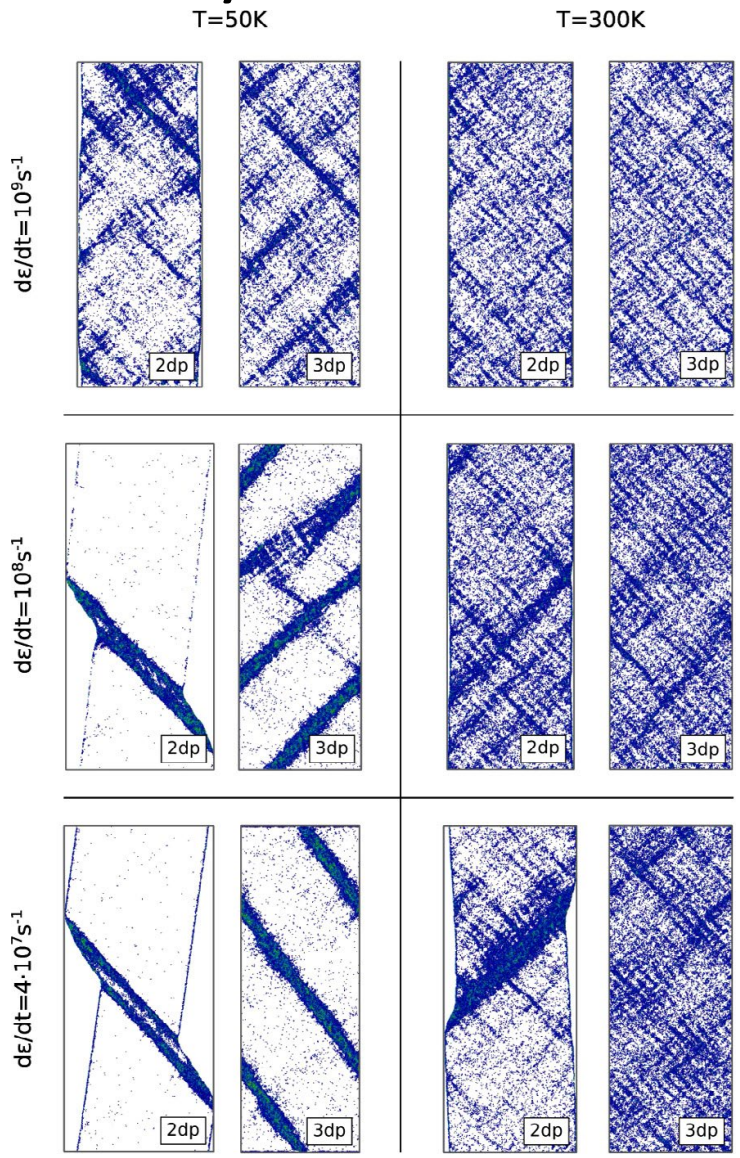

Snapshots for the distribution of local atomic shear strains of the deformed samples at an applied strain of 18%

Albe, Mechanics of Materials, 2013

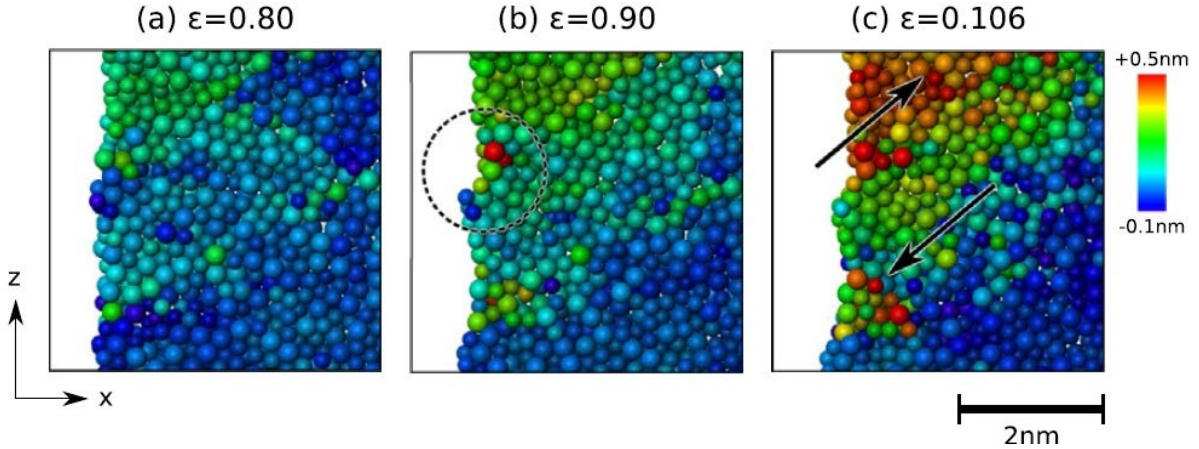

Shear band nucleation at a surface defect resulting from a STZ

(a) at 8% strain, the surface roughness is low, and no surface defects could serve as stress concentrators

(b) at 9% strain, a STZ is activated at the surface and, since STZ operation involves the rearrangement of atoms with volumetric changes, leaves behind a kink (marked by the circle)

(c) at even higher strain, the kink serves as a stress concentrator and leads to shear localization (indicated by arrows), the embryonic SB propagates through the sample and reaches the opposite surface at about 13% strain, when SB slip occurs

Three models—VFT, AM, and MYEGA for viscosity of MG

VFT:

$$\log_{10}\eta(T) = \log_{10}\eta_\infty + \frac{\left(12-\log_{10}\eta_\infty\right)^2}{m\left(\frac{T}{T_g}-1\right)+\left(12-\log_{10}\eta_\infty\right)}.$$

AM:

$$\log_{10}\eta(T) = \log_{10}\eta_\infty + \left(12-\log_{10}\eta_\infty\right)\left(\frac{T_g}{T}\right)^{m/(12-\log_{10}\eta_\infty)}$$

MYEGA:

$$\log_{10}\eta(T) = \log_{10}\eta_\infty + \left(12-\log_{10}\eta_\infty\right)\frac{T_g}{T}\exp\left[\left(\frac{m}{12-\log_{10}\eta_\infty}-1\right)\left(\frac{T_g}{T}-1\right)\right]$$

Chen et. al, Appl. Sci. 2020

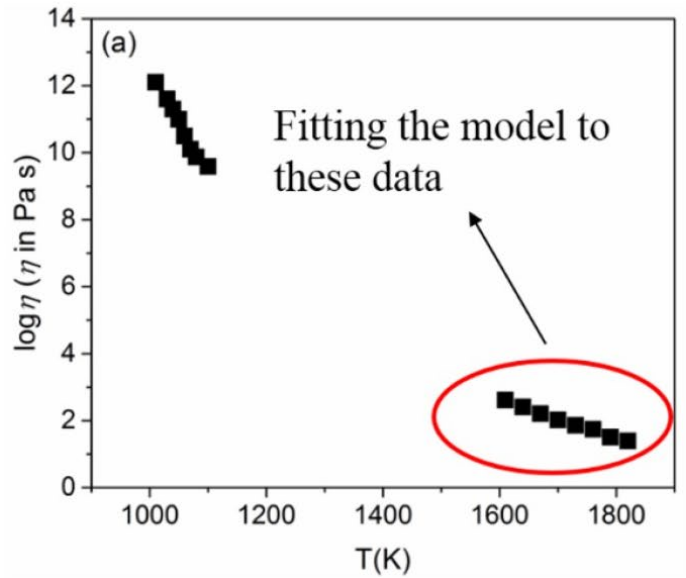

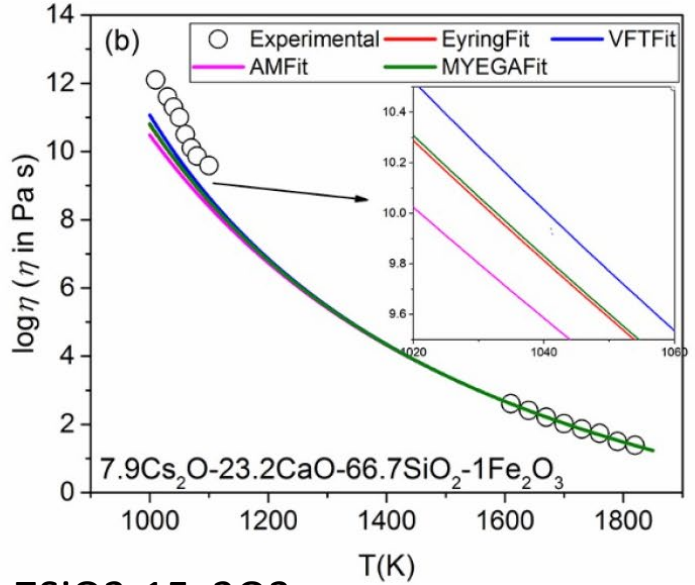

(a) Viscosity data of 7.9Cs2O-23.2CaO-66.7SiO2-1Fe2O3

(b) results of the low-temperature extrapolation of the four models

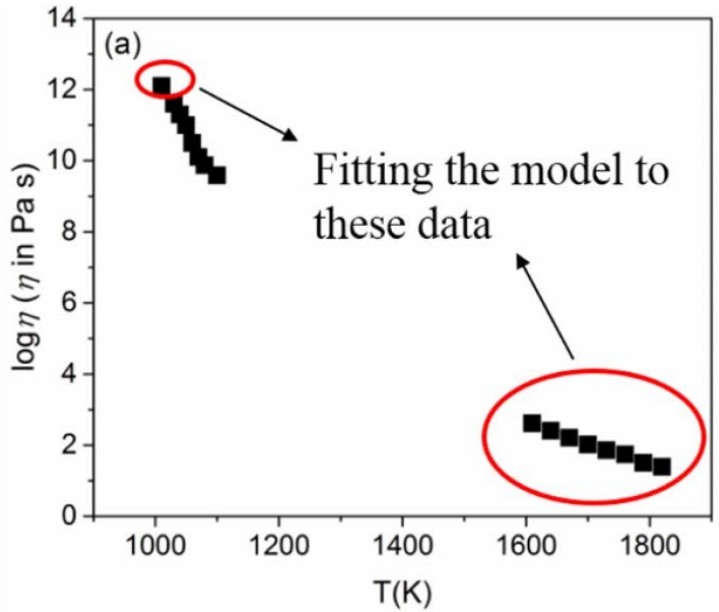

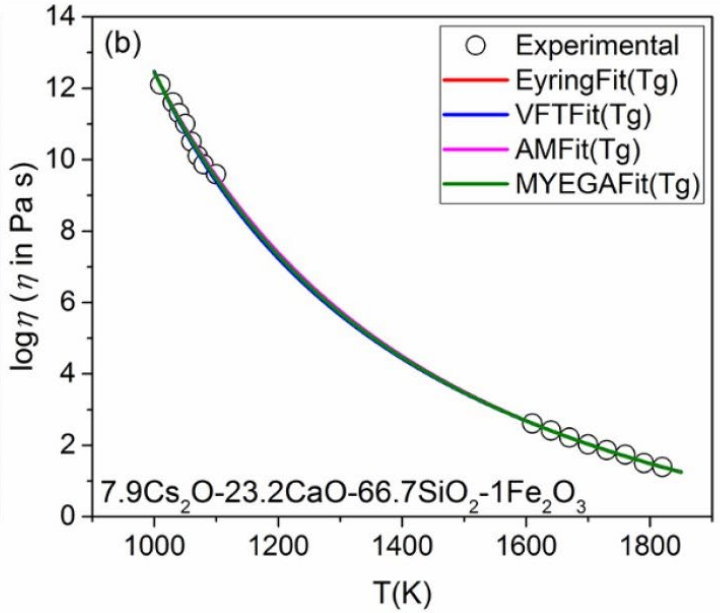

(a) Viscosity data of $7.9Cs_2O$-23.2CaO-66.7SiO_2-1Fe_2O_3 (the data in the red circle are for fitting); (b) results of the low-temperature extrapolation test of the four models.

Chen et. al, Appl. Sci. 2020

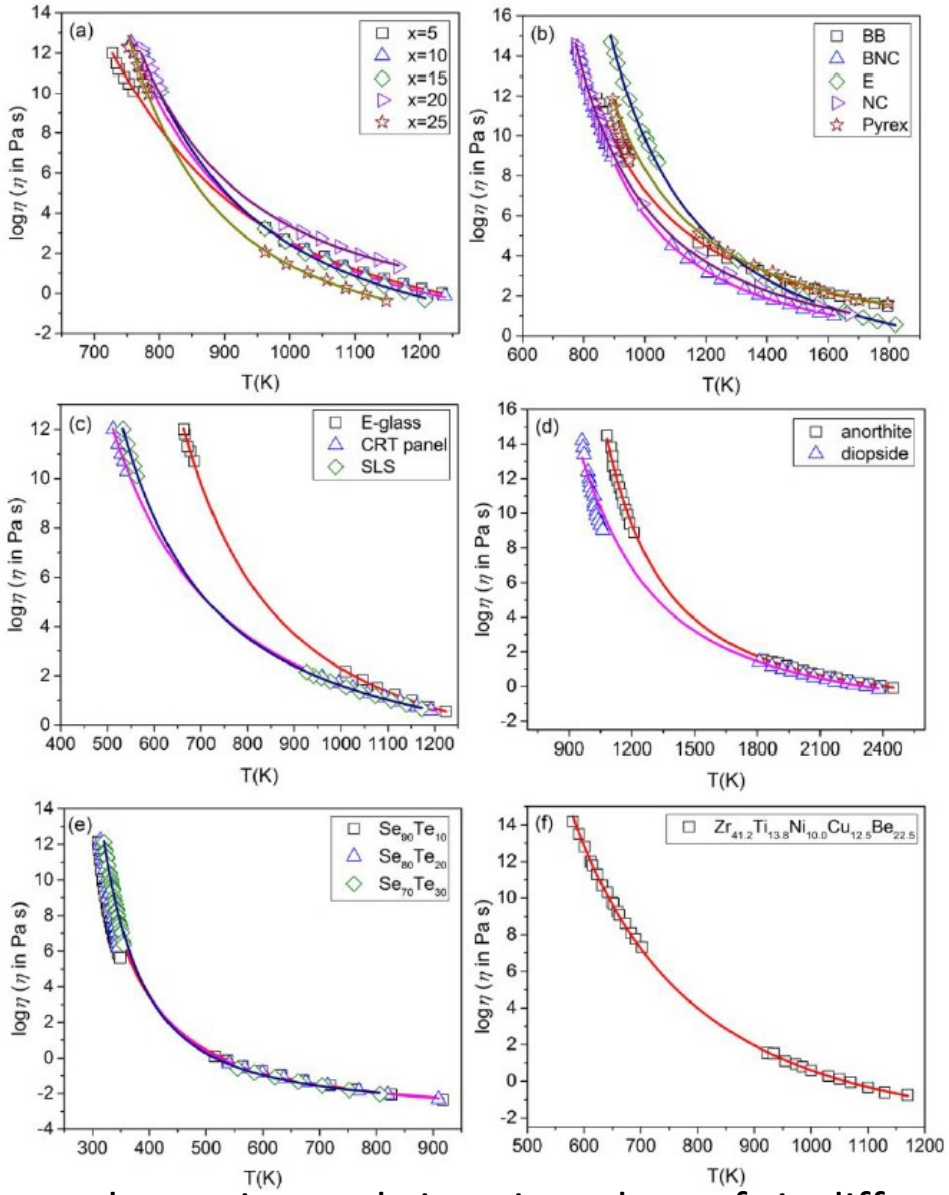

Comparison between predicted values and experimental viscosity values of six different glasses:
(a) xNa2O-10CaO-(89-x)B2O3-1Fe2O3 (x = 5, 10, 15, 20, 25); (b) borosilicate melts; (c) silicate glass foam; (d) anorthite and diopside; (e) Se90Te10, Se80Te20 and Se70Te30 glass-forming system; (f) metallic glass Zr41.2Ti13.8Ni10.0Cu12.5Be22.5.

Chen et. al, Appl. Sci. 2020

Summary

- Amorphous materials are ubiquitous in nature and technology and can be generated by numerous methods
- Amorphous materials have some unique physical, mechanical and chemical properties due to their distinct microstructure, which may be developed for industrial applications
- Amorphization is considered as a new deformation mechanism of materials at high pressure, high strain rates and high strains-the extreme regime

Future work

A review paper on the topic of amorphization by mechanical deformation is in preparation.
Amorphization as a new deformation mechanism at extreme regimes will be studied intensively.
High energy density laser shock compression induced amorphization on some covalently-bonded materials, olivine, forsterite, perovskite and diamond will be analyzed by SEM, TEM and other characterization methods.

Thank you!